

Accelerated Sea-Level Rise Limits Vegetation Capacity to Sequester Soil Carbon in Coastal Wetlands a Study Case in South-Eastern Australia

Steven Sandi¹, Jose Rodriguez¹, Patricia Saco¹, Neil Saintilan², and Gerardo Riccardi³

¹The University of Newcastle

²Macquarie University

³Department of Hydraulics and Research Council of National University of Rosario (CIUNR)

November 23, 2022

Abstract

Estimates of global carbon stocks in coastal wetlands reveal that these are some of the most efficient carbon-sequestering environments in the world, which has prompted a renewed interest in conservation and restoration programs as an opportunity for greenhouse gas abatement. Accumulation of carbon in coastal wetlands is linked to diverse factors such as the type of vegetation, geomorphic setting, and sediment supply. Feedbacks between these factors and the tidal flow conditions drive the dynamics of carbon accumulation rates. Climate change-induced sea-level rise has been shown to increase the vulnerability to submergence of saltmarsh and mangroves in coastal wetlands, even if accommodation and landward colonization are possible. These potential losses of wetland vegetation combined with the reduced productivity of newly colonized areas will directly affect the capacity of the wetlands to sequester carbon from sediments and root growth. Here, we implement an eco-geomorphic model to simulate vegetation dynamics, soil carbon accumulation, and changes in soil carbon stock for a restored mangrove-saltmarsh wetland experiencing accelerated sea-level rise. We evaluate model outcomes for existing conditions and two different management scenarios aimed at mitigating sea-level rise effects and conserve wetland vegetation. Even though some management measures can result in partial conservation of wetland vegetation, they do not necessarily result in the best option for soil carbon capture. Our results suggest that accelerated sea-level can trigger accelerated wetland colonization resulting in wetland areas with limited opportunities for soil carbon capture from sediment and root mineralization, an issue that has not been considered in previous studies.

Accelerated Sea-Level Rise Limits Vegetation Capacity to Sequester Soil Carbon in Coastal Wetlands: a Study Case in South-Eastern Australia

S. G. Sandi¹, J.F. Rodriguez¹, P. M. Saco¹, N. Saintilan², and G. Riccardi³

¹ Centre for Water Security and Environmental Sustainability (CWSES) and School of Engineering, The University of Newcastle, Australia

² Department of Environmental Sciences, Macquarie University, Australia

³ Department of Hydraulics and Research Council of National University of Rosario (CIUNR), Argentina

Corresponding authors: Steven G. Sandi (steven.sandirojas@newcastle.edu.au).
Jose. F. Rodriguez (jose.rodriguez@newcastle.edu.au).

Key Points:

- Wetland losses due to sea-level rise and reduced productivity of newly colonized areas limit soil carbon sequestration
- Focus on conservation of wetland vegetation is not necessarily the optimal option for soil carbon sequestration objectives
- Implementation of eco-geomorphic frameworks is of major importance for adequately quantifying projections of soil carbon stocks

Abstract

Estimates of global carbon stocks in coastal wetlands reveal that these are some of the most efficient carbon-sequestering environments in the world, which has prompted a renewed interest in conservation and restoration programs as an opportunity for greenhouse gas abatement. Accumulation of carbon in coastal wetlands is linked to diverse factors such as the type of vegetation, geomorphic setting, and sediment supply. Feedbacks between these factors and the tidal flow conditions drive the dynamics of carbon accumulation rates. Climate change-induced sea-level rise has been shown to increase the vulnerability to submergence of saltmarsh and mangroves in coastal wetlands, even if accommodation and landward colonization are possible. These potential losses of wetland vegetation combined with the reduced productivity of newly colonized areas will directly affect the capacity of the wetlands to sequester carbon from sediments and root growth. Here, we implement an eco-geomorphic model to simulate vegetation dynamics, soil carbon accumulation, and changes in soil carbon stock for a restored mangrove-saltmarsh wetland experiencing accelerated sea-level rise. We evaluate model outcomes for existing conditions and two different management scenarios aimed at mitigating sea-level rise effects and conserve wetland vegetation. Even though some management measures can result in partial conservation of wetland vegetation, they do not necessarily result in the best option for soil carbon capture. Our results suggest that accelerated sea-level can trigger accelerated wetland colonization resulting in wetland areas with limited opportunities for soil carbon capture from sediment and root mineralization, an issue that has not been considered in previous studies.

Plain Language Summary

Coastal wetlands are environments with a high capacity to transfer carbon from the atmosphere and accumulate it in the soil. Recently, there has been significant interest in promoting conservation and restoration of wetlands as a means to reduce carbon in the atmosphere. Carbon accumulation depends on the complex interaction between tides, vegetation and sediments. Vegetation produces organic matter and slows down the flows which allow sediments to deposit increasing the surface elevation. Because of rapid sea-level rise as a result of climate change, coastal wetlands areas are increasingly vulnerable to submergence. Wetland vegetation will colonize new areas inland to compensate for these losses, but this colonization may be limited by human-made infrastructure. Vegetation losses and limited colonization will result in vegetation with less capacity to accumulate soil carbon. Here, we use a model to study the effects of sea-level rise on vegetation and soil carbon accumulation. We apply the model to a restored mangrove-saltmarsh wetland considering different management scenarios during rapid sea-level rise. Our results suggest that management strategies must integrate the processes described here as management practices can lead to newly colonized vegetation with limited opportunities to accumulate soil carbon.

1 Introduction

Mangroves and saltmarshes are recognized to be some of the most carbon-rich environments found throughout the world (Donato et al., 2011; Ouyang & Lee, 2014). In these coastal environments, carbon stocks (also known as blue carbon) are stored in the form of underlying sediments, the living plant biomass, and the non-living plant biomass (Howard et al., 2014). Different processes including carbon gas emissions, litter fall, sediment entrapment, and dead root mineralization drive the dynamics of soil carbon accumulation in coastal wetlands. Over time, carbon is slowly buried in the soil, which leads to the rich carbon soils underneath the wetlands. Changes in land use of coastal wetlands have occurred over centuries and the effective removal of mangrove and saltmarsh has contributed to

accelerated depletion of soil carbon stocks in the form of gas emissions to the atmosphere (Lovelock et al., 2011; Pendleton et al., 2012; Atwood et al., 2017; Lovelock et al., 2017). This occurs because once wetland vegetation is removed and the land use is converted to other uses (aquaculture, agriculture, shrimp ponds, industrial use, timber harvest, and urban development), sediments are destabilized and or exposed to oxygen which leads to increased microbial activity and gas emissions.

Studies in recent years have addressed the importance of mangrove and saltmarsh conservation as a means to reduce gas emissions (Macreadie et al., 2017a; Adame et al., 2018; Rogers et al., 2019a). Many of these studies have concentrated on estimating current carbon stocks and current rates of gas emissions (Donato et al., 2011; Ouyang & Lee, 2014; Pendleton et al., 2012; Atwood et al., 2017; Thorhaug et al., 2019; Macreadie et al., 2017b), as well as understanding the variability of carbon stocks and the processes that drive the accumulation of carbon (Roner et al., 2016; Morris et al., 2016; Ouyang et al., 2017; Kelleway et al., 2017a; Pérez et al., 2018; Kusumaningtyas et al., 2019; Abbott et al., 2019). The effects of sea-level rise on carbon sequestration dynamics and current stocks have only recently started to be considered (Rogers et al., 2019b; Watanabe et al., 2019; Breithaupt et al., 2020) and initial findings seem to indicate potential increases in carbon accumulation by the end of the century, at least in some scenarios of increased CO₂ emissions (Krauss et al., 2017; Wang et al., 2019).

The full effects of sea-level rise on soil carbon accumulation, however, remain uncertain (Kirwan & Mudd, 2012; Lovelock & Reef, 2020). In coastal wetlands, particularly in mangroves and saltmarsh, complex eco-geomorphic feedbacks between sediment transport, water flow, and vegetation strongly affect the dynamics of the system. Models that can include these feedbacks, especially between vegetation and soil processes (Kirwan & Magonigal, 2013; Kirwan et al., 2016; Saco & Rodríguez, 2013) and hydraulic effects (Passeri et al., 2015; Lentz et al., 2016; Alizad et al., 2016a), are of major importance for adequately representing the dynamics of the wetland and potential changes in the future (Passeri et al., 2015; Rodríguez et al., 2017). For instance, mangrove landward colonization under contemporary sea-level rise rates can result in increased blue carbon sequestration of wetlands due to the higher carbon sequestration capacity of mangroves compared to other vegetation (Krauss et al., 2017; Kelleway et al., 2016; Lamont et al., 2020); however, under future rates of sea-level rise wetland losses due to submergence are expected (Kirwan et al., 2016; Craft et al., 2009; Lovelock et al., 2015; Ward et al., 2016), which can balance out or surpass carbon sequestration gains due to landward colonization. In addition, the presence of human-made structures within the wetlands (Rodríguez et al., 2017; Sandi et al., 2018) and barriers to wetland colonization (Schuerch et al., 2018) limit the capacity for wetlands to adapt to future sea-level rise. More importantly, rapid retreat and colonization triggered by accelerated changes in sea-level may not allow vegetation to mature, resulting in newly colonized areas with different vegetation structure, affecting the soil carbon accumulation dynamics (Krauss et al., 2017). The inclusion of soil carbon dynamics in an eco-geomorphic modelling context allows us to track wetland accretion, retreat, and transgression, which can then be used to estimate the potential vulnerability of soil carbon stocks and carbon accumulation rates in coastal wetlands.

The issue of future soil carbon sequestration potential of coastal wetlands is of extreme importance for wetland restoration projects. For centuries, the imposition of levee banks has isolated wetlands from tidal inundation and facilitated their conversion to agricultural land. A recognition of the habitat values of wetlands and their declining extent across the globe has prompted the “de-embankment” and managed realignment of saltmarshes in the UK Essex and Norfolk coastlines (Mossman et al., 2012), the Baltic Sea

saltmarshes in northern Germany (Hofstede, 2019), and other initiatives driven by the EU Habitats Directive. Similar restoration projects in North America and Australia have been funded through compensatory habitat schemes, with tidal reinstatement facilitating the restoration of the vegetative and hydrological requirements of bird and fish habitat (Elphick et al., 2015; Boys & Pease, 2017). Increasingly, tidal reinstatement is seen as a leading opportunity for greenhouse gas abatement, providing a financial incentive to the restoration of “blue carbon” ecosystems (Kroeger et al., 2017; Sheehan et al., 2019; Kelleway et al., 2020). The long-term success of these projects will depend on how wetlands respond to sea-level rise, both in terms of the extent of vegetated habitat and in the continuity and efficacy of ecosystem services, including soil carbon sequestration. In these restored systems, the nature of entrance conditions, particularly the hydrodynamic constraints imposed at the point of levee removal, may prove to be a critically important determinant of end-points, both in terms of habitat extent and the volume of soil carbon sequestered. These two restoration objectives (i.e. optimal habitat restoration and optimal soil carbon sequestration) may not be mutually attainable, as it is often assumed.

Here we extend an eco-geomorphic model of coastal wetlands that simulates hydrodynamic and vegetation processes (Rodríguez et al., 2017; Sandi et al., 2018) to incorporate soil carbon processes. This simulation approach integrates a detailed hydrodynamic model that fully integrates attenuation effects due to natural and human-made features, vegetation response based on their preference to hydrodynamic conditions, and bio-geomorphic accretion (Morris et al., 2002; Kirwan et al., 2010). We apply this model to a wetland in the Hunter Estuary, Australia, where tidal flows have been reinstated. Restoration of the wetland has provided important habitat areas for shorebirds, but predictions of future losses of wetland vegetation under sea-level rise have prompted analysis of management alternatives based on inlet control (Rodríguez et al., 2017; Sandi et al., 2018). We estimate the current stock of soil carbon based on measurements at the site (Howe et al., 2009) and we simulate changes in the soil carbon stock under sea-level rise by accounting accreted carbon and contributions from biomass production via root mineralization as well as potential carbon losses under three different management scenarios: 1) no tidal gate control; 2) tidal gate at a fixed elevation; and 3) tidal gate at an elevation changing with SLR. In all management scenarios surrounding earthworks and embankments impede landward colonization.

1.1 Study area

This research focuses on Area E, an enclosed rehabilitated wetland site situated in Kooragang Island, New South Wales, Australia, approximately 10.5 km from the mouth of the Hunter River (Fig. 1a) with a total area of 1.24 km². Wetlands of the Hunter Estuary are of major importance for migratory shorebirds. In the past, many areas of the estuary including Kooragang Island (Fig. 1) were drained using a series of levees and culverts to make the land suitable for cattle grazing, logging and industrial use. In the 1990s, tidal flows were reinstated in Area E to restore wetland areas (Williams et al., 2000). Reinstatement of tidal conditions promoted landward colonization of estuarine communities and allowed mangroves to colonize shallow mudflats, tidal pools and low elevation saltmarsh habitats (Howe et al., 2010). This type of mangrove vegetation transgression has been reported for many other sites in NSW (Saintilan & Williams, 1999; Saintilan et al., 2014) and it can lead to a general loss of wetland biodiversity (Kelleway et al., 2017b).

The site includes most of the estuarine habitats present in the Hunter Estuary (Howe et al., 2010), including mudflats, tidal pools, mangroves and saltmarsh. Mangrove forests are composed of Grey Mangrove (*Avicennia marina*) and saltmarshes are dominated by Beaded Samphire (*Sarcocornia quinqueflora*) and Marine Couch (*Sporobolous virginicus*). The study

area receives flows directly from the South Arm of the Hunter River where the hydrodynamics are dominated by the tidal regime as runoff flows coming from the Hunter River are comparatively small. The tidal regime follows a semi-diurnal tidal cycle with a tidal range of about 1.6 m.

In Australia, mangrove commonly occupies the lower elevations of the upper intertidal zone and saltmarsh is usually found at higher elevations (Rogers & Krauss, 2019). On occasions, such as the case of Area E, mudflats can be present in the lowermost areas of the intertidal range. The human-made structures within and surrounding Area E limit accommodation i.e. the vertical and lateral space available for fine sediments to accumulate and be colonized by wetland vegetation. This poses a threat to saltmarsh as mangroves are expected to continue encroaching on the saltmarsh areas in the future (Rodríguez & Howe, 2013). At the same time, submergence of wetland vegetation under sea level rise is also expected to occur (Rodríguez et al., 2017; Sandi et al., 2018).

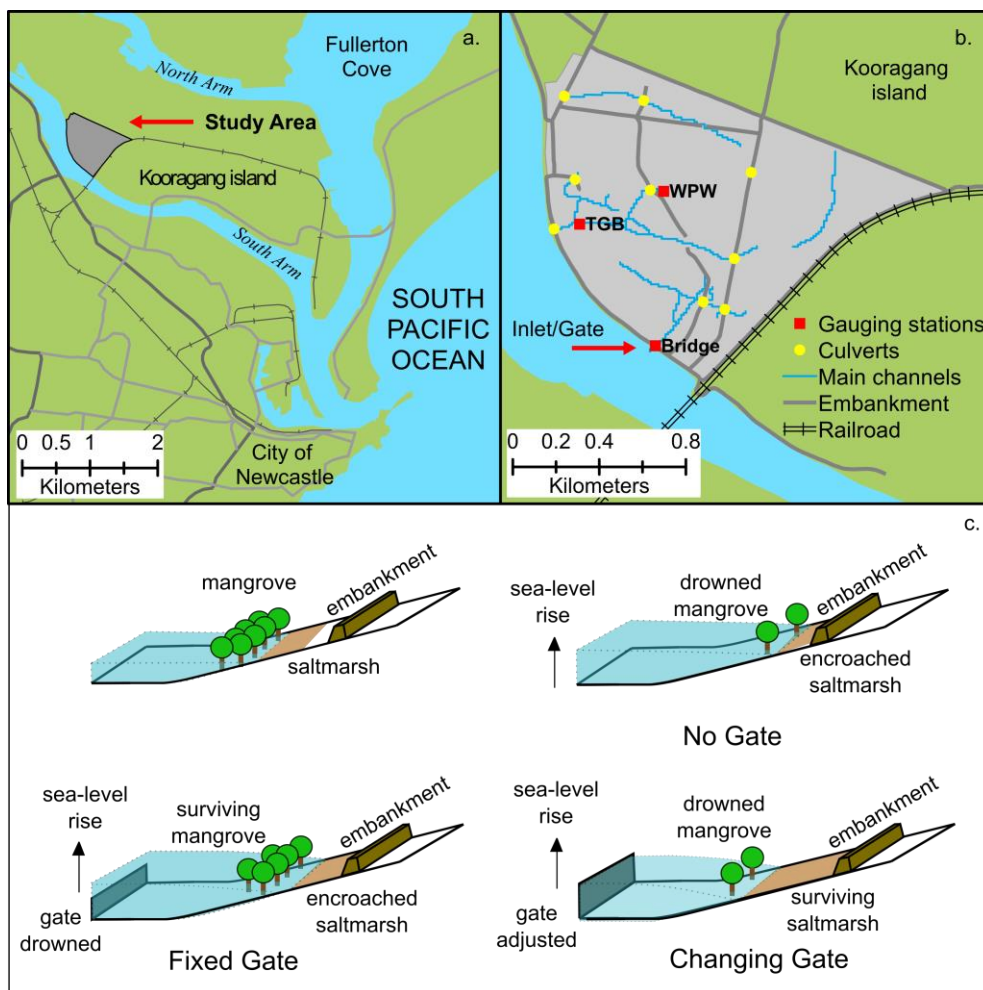


Figure 1. Location the study area (a), and details of the site configuration including internal and surrounding infrastructure and drainage network (b), schematic of the different control scenarios (c). Earthworks and embankments impede landward colonization. Sea level rise corresponds approximately to projections after 100 years.

2 Materials and Methods

In order to simulate potential effects of sea-level rise on the soil carbon of Area E, we first estimate the recent soil carbon stock based on-site measurements. We then investigate the potential changes in the soil carbon stock by simulating the eco-geomorphic feedbacks between vegetation, tidal regime, and sediment accretion under sea-level rise using the methodology developed by Rodríguez et al. (2017) and Sandi et al. (2018). This allows estimating the changes in vegetated areas of mangrove and saltmarsh as well as the changes in surface elevation due to bio-geomorphic accretion. We also account for changes in the biomass productivity that contributes to the soil carbon. We then incorporate specific rates of change in the soil carbon to represent potential carbon losses arising from root mineralization and vegetation loss.

This eco-geomorphic approach includes different models operating at different timescales. First, a spatially distributed hydrodynamic model provides a detailed long-term description of the tidal regime that drives the establishment and decline of mangrove and saltmarsh. The vegetation distribution is coupled with a bio-geomorphic accretion model used to update the topography. Both vegetation distribution and changes in surface elevations are re-incorporated into the hydrodynamic model to provide feedback directly into the simulation through updated hydraulic resistance and topography. For simulating sea-level rise, the input water levels, surface elevation change, and vegetation characteristics are updated according to the sea-level rise projection every 20 years (see section 2.5).

Once changes in vegetation and surface elevation are estimated, the changes in soil carbon stock are calculated by considering the sequestered carbon through organic sediment deposition obtained as a fraction of the simulated accreted soil and also including inputs from dead root mineralization. If vegetation is lost due to submergence, we assume that aboveground biomass productivity is lost, and a fraction of the below-ground biomass production becomes soil carbon, but the capacity to continue accumulating soil carbon is lost. Potential changes of carbon in living biomass are not accounted for, but changes in the vegetation are tracked in all simulations.

We implement our modelling approach to assess the potential effects of sea-level rise in the soil carbon stock of the wetland and sequestering capacity under different management scenarios using inlet control. We first consider a scenario with no control at the inlet in Fish Fry Creek (Fig. 1b), which represents a baseline scenario. The other two scenarios are considered by introducing a hydraulic control gate at the Fish Fry Creek inlet. This control gate has been proposed to limit mangrove encroachment on saltmarsh, one of the main consequences of sea-level rise that compromises shorebird habitat (Howe et al., 2010; Rodríguez & Howe, 2013). We consider a fixed gate scenario with a level of 0.35 m above Australian Height Datum (mAHD) and a rising gate scenario with the gate level starting at 0.35 mAHD and gradually rising the gate level following the rising sea-level. Similar control scenarios were implemented by Sandi et al. (2018) to assess the effectiveness of the control structures in preserving bird habitat. The gate produces attenuations to the tidal regime, only allowing the tide levels above the gate level to enter the wetland. The gate also has the effect of increasing inundation duration of mangrove areas, limiting mangrove encroachment. Earthworks and embankments impede landward colonization. In the fixed gate scenario, the gate eventually becomes drowned and attenuation effects are reduced so mangrove can encroach on saltmarsh (Fig. 1c), but in the rising gate scenario the attenuation of the tidal input is maintained, which continues limiting mangrove encroachment and promotes saltmarsh survival (Fig. 1c).

2.1 Hydrodynamic model

The flow regime is modelled with a quasi-2D hydrodynamic model, developed for describing wetting and drying processes in floodplain systems (Riccardi, 2000) affected by flow resistance. The model structure is based on an interconnected cells scheme and uses simplified versions of the shallow flow equations to determine the water depths in the wetland. Full dynamic equations are used for channel flow, but for slow floodplain flows, in which inertial effects can be neglected, a diffusive wave simplification is used, speeding up computations. The model includes formulations to simulate flow through culverts, embankments, earthworks and control gates. The simulated domain is discretized into a 10 m resolution squared grid with a total of 13543 cells. Boundary conditions at the wetland entrance (Fish Fry Creek and Wader Creek inlets in Fig. 1b) consist of water surface elevations in the Hunter estuary. The resulting differential equation system is solved with a two-dimensional finite differences scheme using a Gauss-Seidel iteration method where the Courant-Friedrichs-Lewy celerity condition is used for stability of the model. Calibration and model testing has been previously presented by Rodríguez et al. (2017) and Sandi et al. (2018) (see Supplementary Materials for comparison plots and performance indicators).

Previous models of soil carbon dynamics do not consider the effects of flow resistance, tidal attenuation or human-made structures. For comparison purposes, we also run simplified calculations considering that the flow dynamics in the wetland are unaffected by structures or vegetation. Water levels in all points of the wetland are considered the same as the water level of the tidal data at the inlet. We refer to this as the “bathtub approach” and it is strictly a simplification of the flow dynamics. Vegetation and accretion are estimated the same way as in the hydrodynamic approach. Recent literature advocates for a shift from using bathtub approaches to models that can include non-linear responses of the vegetation to hydrodynamics and coastal morphology (Passeri et al., 2015). Bathtub models can underestimate coastal wetland vulnerability, resulting in less wetland submergence from simulations (Rodríguez et al., 2017). This can have significant implications in the simulation of sequestered soil carbon, so we use the results of the bathtub model to explore the magnitude of soil carbon accumulation in comparison to a hydrodynamic approach. Results of wetland vegetation extent, biomass productivity and accretion using the bathtub model are presented in Supplementary Material.

2.2 Vegetation

We simulate the vegetation by first calculating spatially distributed time-aggregated variables of the tidal regime from the hydrodynamic simulations. Rules for vegetation establishment can be described by suitable ranges of depth below mean high tide (D) and the ratio of inundated time over total time or hydroperiod (H) (Kirwan et al., 2010; D'Alpaos et al., 2007; Kirwan & Murray, 2007). Here, values of D and H were obtained integrating spring tide results from one year of continuous hydrodynamic simulations as in Rodríguez et al. (2017) and Sandi et al. (2018). During spring tides, water levels and inundation extent are more pronounced and become critical for vegetation establishment and survival in the upper intertidal frame (Howe, 2008).

Mangrove establishment is strongly influenced by hydroperiod (Woodroffe et al., 2016). Soils regularly inundated, such as those in estuarine environments, can experience an accumulation of phytotoxins (McKee, 1993; Youssef & Saenger, 1998) or undergo conditions of limited oxygen availability for root uptake (McKee, 1996), thus mangrove species require a minimum period of time for soils to be well aerated and for pneumatophores to obtain enough oxygen. The dominant mangrove species in the site (*Avicennia marina*) is

sensitive to spring-tide hydroperiod, and a suitable range $0.1 < H < 0.5$ was adopted based on data collected on site (Howe, 2008). A similar hydroperiod range for *Avicennia marina* was assumed by van Maanen et al. (2015) for simulating evolution of mangroves in sandy tidal embankments. The range selected by van Maanen et al. (2015) is based on observation of the position of *Avicennia marina* on the intertidal range (Clarke & Myerscough, 1993). This range of hydroperiod is also consistent with simulated data from Crase et al. (2013), for *Rhizophora stylosa*, a mangrove species that occupies a similar position in the tidal range in tropical locations. Though hydroperiod drives mangrove establishment, mangroves are capable of colonizing areas with a wide range of inundation frequencies as other drivers affect suitability conditions necessary for mangroves to grow (Krauss et al., 2008). We also impose a secondary constraint in terms of D and we assume that mangrove propagule establishment is restricted by high soil salinity conditions that will occur under very low values of D (Saintilan et al., 2009). A restriction of $D > 0.2$ m was considered for mangrove suitability conditions.

In Area E, the typical height of dominant saltmarsh species is close to 25 cm; therefore, a limit of $D < 0.25$ m was set for saltmarsh suitability as D that cover the plants completely will drown saltmarsh and result in hypoxia, restricting their establishment (Morris et al., 2002). For saltmarsh, a limit for hydroperiod ($H < 0.8$) was also included to represent that saltmarsh would not establish in areas that are almost permanently inundated. Finally, saltmarsh was assumed to be outcompeted by mangrove in wetland areas with adequate conditions for both species, as reported in previous work (Saintilan et al., 2014).

The vegetation model was tested by comparing the simulated vegetation distribution against a vegetation map obtained by combining RTK GPS data and a ground-truthed high-resolution aerial photography for the year 2007 (Howe, 2008). The simulated vegetation is obtained by running the hydrodynamic and vegetation models using as input the tidal information of 2007 from a nearby gauging station (see Supplementary Materials for comparison maps and performance indicators).

2.3 Eco-geomorphic accretion model

In order to include changes in soil surface elevation for long-term projections of sea-level rise, a previous methodology based on saltmarshes in the US was adapted (Morris et al., 2002; Kirwan et al., 2010). Our model calculates the surface elevation change over time (dE/dt) at each point in the wetland and includes the contribution of suspended sediment deposition and biomass accretion:

$$\frac{dE}{dt} = SSC(q + kB)D \quad [1]$$

where SSC is the suspended sediment concentration q is a depositional parameter that represents the rate at which sediment settles in the absence of vegetation, k represents the efficiency of specific vegetation to trap sediment as well as changes in elevation from organic matter accumulation, and B is the aboveground biomass production. For aboveground biomass production we use the formulation of Morris et al. (2002), where B increases with D until it reaches an optimum value, beyond which biomass production decreases:

$$B = aD + bD^2 + c \quad [2]$$

The parameters a , b and c are determined empirically from site data and are different for saltmarsh and mangrove. Equation 2 satisfies the ecological principle that the vegetation is distributed over a range of tolerance values from different stressors depth (Morris et al., 2002), which in this case is D . In areas with lower D , plants are smaller which means lower biomass production whereas in areas with higher D plants are larger, but there is more competition leading to reduced access to resources and less dense vegetation. Because of this, there should be an intermediate range of flooding where biomass production has the highest values. We calibrated the parameters in equations 1 and 2 using simulated values of D , accretion rate data collected in the study area (Rogers et al., 2013) and, in the absence of biomass production measurements, we adopted biomass values collected in the Georges River for the same dominant vegetation, i.e. saltmarsh and young mangroves less than 15 years old (Kelleway et al., 2016). In the study area, tallest saltmarsh are located at lower elevations so it is assumed that biomass increases as to a maximum value of D , similarly to observations of saltmarsh in South Carolina (Morris et al., 2002). For mangroves, average B was set to the average simulated value of D as it is assumed that small trees will establish in less inundated areas with low D and also more competition will occur in more inundated areas with high D , leading to less productivity. We assume the initial values of biomass production to be the same as the initial biomass to estimate the initial living biomass carbon stock (Table 1). However, because equation 2 allows to estimate primary production but not woody biomass accumulation we do not compute carbon stocks in living biomass over the whole simulation period (see section 2.4.2). Instead, we only consider the cumulative contribution of biomass to the soil carbon via root mineralization, which is calculated as a fraction of the belowground biomass primary production (see section 2.4.1).

The value of SSC is spatially variable and we have assumed a relationship based on measurements from Howe (2008) in which SSC decreases linearly with D from a maximum constant value SSC_{max} at the inlet ($37 \text{ g} \cdot \text{m}^{-3}$). The same relationship was applied by Rodríguez et al. (2017) and Sandi et al. (2018):

$$\frac{SSC}{SSC_{max}} = 0.55D + 0.32 \quad [3]$$

with D in metres. Previous research has used physically-based transport equations for SSC (D'Alpaos et al., 2007; Breda et al., 2020) or an exponential decay formulation with distance to tidal channels (D'Alpaos et al., 2007; Kirwan & Guntenspergen, 2010; Kirwan & Murray, 2008). Because of the complex flow paths within our study area, implementing a physically-based or distance-based model was impractical due to the computational requirements.

The eco-geomorphic accretion model does not consider erosion. Fluvial erosion has not been identified as an important process in the study area for long-term simulations as the stream network has remained stable for many years (Howe, 2008) and episodic storm events have shown reworking of sediments in the vegetated areas rather than net erosion (Rogers et al., 2013). It is assumed that flow within the wetland is slow and vegetation stabilizes sediment and prevents erosion. Erosion by wind waves is limited by the small size of permanent pools and shading effects of infrastructure under current conditions (Howe, 2008), but may become more important as sea-level rises and permanent water pools increase their size (Carniello et al., 2011; Leonardi et al., 2016). However, it is likely that wetland submergence due to the limited accretion capacity of the attenuated system will still be the dominant mechanism of wetland loss during sea-level rise (Ravens et al., 2009) as opposed to erosion.

The calibration of the eco-geomorphic accretion model consisted in obtaining the parameters that produced the best match of the results of equation 1 with local data comprising a 10-year record (2002-2012) of surface elevation changes derived from Surface Elevation Tables (SET) (to ± 1.4 mm) (Howe et al., 2009; Rogers et al., 2013). The calibrated parameters of the eco-geomorphic accretion model (q and k in equation 1 and a , b and c in equation 2) are presented in the Supplementary Material.

2.4 Soil carbon model

Our conceptual model of soil carbon sequestration processes is presented in Fig. 2. The soil carbon stock receives carbon inputs from sediments and litter fall in the topsoil surface layer and from dead root turnover along the soil profile. Part of the soil carbon originating from dead roots is potentially lost by mineralization in the form of gas emissions or dissolved carbon. Our assessment of soil carbon dynamics under sea-level rise considers the organic carbon deposited in the soil due to bio-geomorphic accretion and potential changes in living biomass which translate on buried carbon from root mineralization and carbon losses due to biomass losses and root mineralization.

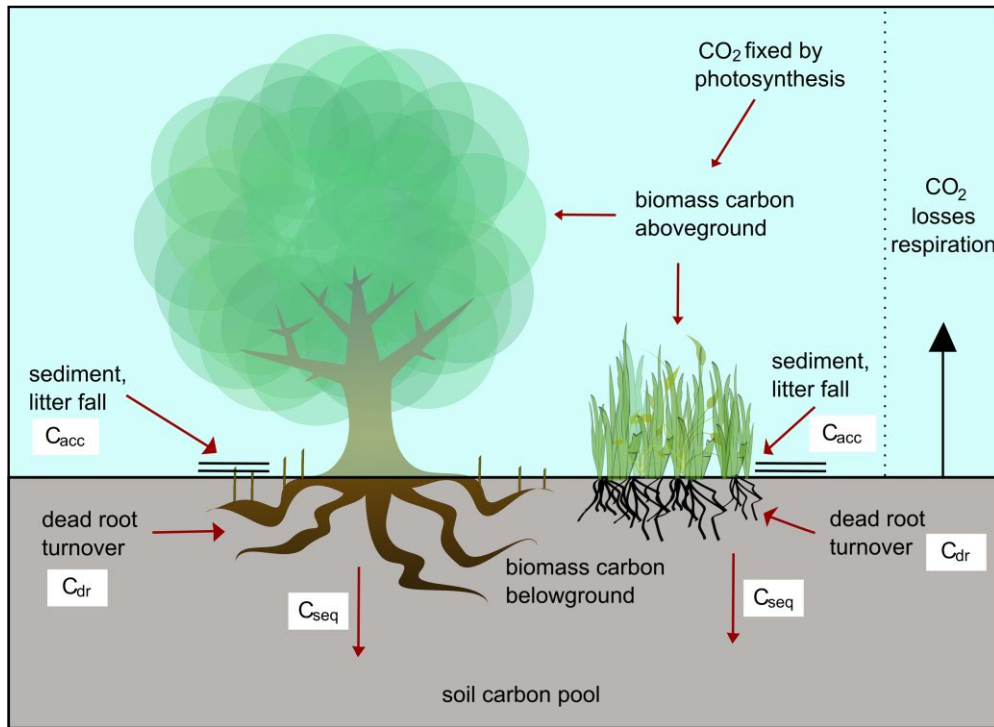


Figure 2. Conceptual carbon sequestration cycle at the site. C_{acc} : accreted carbon, C_{dr} : dead root turnover carbon, C_{seq} : sequestered carbon (sum of C_{acc} and C_{dr}).

2.4.1 Soil carbon stock

The soil carbon stock of a wetland is the sum of all carbon in the soil. We first estimate the contemporary soil carbon stock of Area E considering only the sum of carbon contained in the top 1 m layer of the soil which is standard for a carbon stock inventory (Howard et al., 2014). Also, soil carbon profiles in Kooragang Island show that the majority of the carbon are within this layer (DPI, 2008; Saintilan et al., 2013) and decreases exponentially with depth. This estimate of soil carbon stock is a baseline for comparison, but environmental history is also key in soil carbon accumulation and may not directly reflect the

contemporary vegetation (Kelleway et al., 2017a), especially in the case of mangroves as they were recently established in the study area.

Soil carbon densities (ρ_{sd}) in Area E were obtained for the top 20 cm of the top soil layer of different vegetated and non-vegetated areas by extracting 45 different soil cores (Howe et al., 2009) (see Supplementary Material). Mean organic soil carbon densities were $0.0406 \pm 0.010 \text{ MgC} \cdot \text{m}^{-3}$ ($n = 19$) for saltmarsh, $0.0287 \pm 0.009 \text{ MgC} \cdot \text{m}^{-3}$ ($n = 9$) for mangrove, and $0.0193 \pm 0.006 \text{ MgC} \cdot \text{m}^{-3}$ ($n = 8$) for unvegetated tidal pools and mudflats. Synthetic organic carbon profiles were then estimated to a depth of 1 m using an exponential relationship obtained from carbon profiles in Kooragang Island (See Supplementary Material):

$$\rho'_{sd} = k_0 \cdot e^{-\lambda \cdot z} \quad [4]$$

where ρ'_{sd} is the projected soil carbon density at a depth z in meters from the surface, k_0 is a constant adjusted to the carbon density of the top soil layer (ρ_{sd}) and λ is a decay constant equal to 3.5.

2.4.2 Carbon in biomass

Organic biomass carbon was obtained by first calculating the biomass productivity above and belowground and then converting the living biomass to carbon. We calculate aboveground biomass production using equation 2 which is then converted to aboveground biomass carbon productivity rate (C_{ab}) using a carbon content factor F_1 :

$$C_{ab} = F_1 \cdot B \quad [5]$$

We used the same value $F_1 = 0.47$ for mangrove and saltmarsh as recommended by Kauffman and Donato (2012) and Howard et al. (2014) and in line with biomass carbon content measurements by Owers et al. (2018) in the region of our study area. A similar aboveground biomass carbon content factor was reported for *Spartina alterniflora* saltmarsh in South America (Negrin et al., 2012).

Calculation of carbon produced in belowground biomass follows a similar process to aboveground biomass. To estimate belowground biomass production, we convert B (equation 2) to belowground biomass by adopting an aboveground/belowground biomass factor F_2 . The belowground biomass carbon production rate (C_{bb}) is then computed using a third factor F_3 of carbon content:

$$C_{bb} = F_2 \cdot F_3 \cdot B \quad [6]$$

For mangrove, the value of F_2 is considered to be variable, as observations of mangrove in the region have shown increasing F_2 with increased soil salinity (Saintilan, 1997; Saintilan, 1998). Here, we consider that F_2 increases from 0.5 to 2.0 with decreasing D (accounting for salinity increases) following a power law. This means that areas with lower D are more saline and the F_2 factor is higher. For F_3 , we follow Howard et al. (2014), who proposes a value of $F_3 = 0.39$ for mangrove based on Jaramillo et al. (2003). For saltmarsh, values of $F_2 = 0.5$ and $F_3 = 0.34$ were selected as recommended by Howard et al. (2014) based on Duarte (1990).

The initial living biomass carbon stock (Table 1) is assumed to be equal to the sum of biomass production rates (C_{ab} and C_{bb}) at the beginning of the simulation when there are newly established mangroves and saltmarsh in the study site. However, biomass carbon stocks are not computed over time as our model does not compute the accumulation of woody biomass in mangroves.

2.4.3 Soil carbon accumulation rates

We compare the capacity of the wetland to sequester soil carbon between the three different control scenarios by estimating the carbon accumulation rate per area (C_{seq}). We define this rate as the sum of the accreted carbon rate and the rate of carbon buried from dead root decomposition:

$$C_{seq} = C_{acc} + C_{dr} \quad [7]$$

We calculate the accreted carbon rates (C_{acc}) in each cell of our model by multiplying the surface elevation change (equation 1) by the top soil organic carbon density:

$$C_{acc} = \rho_{sd} \cdot \frac{dE}{dt} \quad [8]$$

This accreted carbon is added to the soil carbon stock. The carbon produced in the living biomass is represented by C_{ab} and C_{bb} (equations 5 and 6), and it is recalculated every 20 years, at time when we update tidal levels, soil surface elevation, vegetation distribution and biomass production due to sea-level rise. Turnover of carbon stored in roots originating from belowground biomass production (C_{bb}) is added annually over time to the soil carbon stock. Most of the mineralized carbon from dead roots is lost as pore water or gas emissions, but a considerable amount remains buried in the soil. Ouyang et al. (2017) estimate that dead root burial accounts for 24% - 29% of the annual sequestered carbon in mangroves and 77.9% of the annual carbon sequestered in saltmarsh. The rate at which carbon is buried in the soil as a result of dead root decomposition C_{dr} is calculated as:

$$C_{dr} = C_{bb} \cdot P_{dr} \cdot (1 - k_d) \quad [9]$$

where P_{dr} is the dead root productivity rate with values of 0.22 year⁻¹ for mangrove and 0.67 year⁻¹ for saltmarsh and k_d is the root decay rate, with values of 0.493% year⁻¹ for mangrove and 0.434% year⁻¹ for saltmarsh (Ouyang et al., 2017; Bouillon et al., 2008; Alongi, 2014).

Initial soil carbon accumulation rates are different for the gate-controlled scenarios as the inclusion of a gate affects the distribution of the vegetation.

In addition, we do not explicitly calculate potential inputs of soil carbon originating from aboveground dead biomass; however, carbon inputs from litter fall and suspended organic matter are included in the accreted carbon which comes from bio-geomorphic accretion (equation 1).

2.4.4 Potential carbon losses

For comparison of potential carbon losses between scenarios, we consider different processes of carbon loss when vegetation is submerged or replaced due to sea-level rise. In

our assessment, changes in vegetation are quantified every 20 years, so we also estimate potential carbon losses every 20 years. We assume if vegetation is submerged or replaced by another vegetation, the carbon not mineralized from belowground biomass will be lost. We also consider that there are no losses from carbon stored in the soil when vegetation is submerged because we assume that the soil will remain relatively undisturbed during this process (Krauss et al., 2018; Negandhi et al., 2019). When vegetation survives 20 years under sea-level rise, the fraction of carbon not mineralized from dead root biomass is added to the potential carbon losses annually over time. Cumulative potential carbon losses are converted into CO₂ to represent greenhouse gases emissions, assuming all emissions occur as CO₂, although carbon losses can also occur in the form of CH₄ or carbon dissolved in water. Similarly, the cumulative sequestered carbon estimated by our model will be converted to CO₂, as this will represent the potential greenhouse gases burial in the study area under each scenario.

Different practices that lead to wetland vegetation losses, such as wetland conversion to grazing, aquaculture, shrimp ponds or other land uses, can lead to significant losses of soil carbon because soils are highly disturbed as part of these practices (Atwood et al., 2017). In this research, only vegetation losses due to sea-level rise are considered, and future carbon losses originating from wetland conversion should receive special considerations.

2.5 Sea-level rise projections

To calculate the future potential dynamics of the soil carbon stocks, we consider an accelerated rate of sea-level rise the next 100 years following the RCP8.5 scenario of the IPCC Fifth Assessment Report (Church et al., 2013). We considered increasing rates of sea-level rise from 4 mm·yr⁻¹ in recent time up to 11 mm·yr⁻¹ by the end of the century. The rates of sea-level rise are increased every 20 years, at the time where the tidal input, surface elevations, and characteristics of the vegetation are updated and integrated into the hydrodynamic model to simulate feedback effects. Similarly, Alizad et al. (2016a) and Alizad et al. (2016b) implemented a methodology where rates of sea-level rise were increased in time-steps for simulations of saltmarsh in the Florida panhandle. Their time-steps were shorter than ours (5 to 10 years), but this was because their rates of sea-level rise were larger. The initial rate of sea-level rise in our study site was corroborated with data from the Hexham Bridge gauging station located 1 km upstream of the wetland site. Changes in the amplitude of the tidal series were not considered as the same data from the Hexham bridge show no change in the amplitude over the last 10 years. We limit the analysis to the RCP8.5 scenario because is the scenario where more changes in vegetation would be expected, which means it can provide the highest contrast of soil carbon sequestration for the control scenarios in our simulation period. Recently updated projections of sea-level rise from the IPCC Special Report on the Ocean and Cryosphere in a Changing Climate also use the RCP8.5 scenario (Oppenheimer et al., 2019). The latest projections show higher rates of sea-level rise in comparison to the IPCC Fifth Assessment Report, but our assumed values are within the likely range of the latest projections.

3 Results

3.1 Initial soil carbon stock

Our estimate of the soil carbon stock in the top 1 m layer shows that the largest soil carbon per unit area corresponds to saltmarsh (Table 1). The soil carbon content per area in saltmarsh areas is 40% higher than in mangroves and 120% higher than in mudflats. As

saltmarsh also covers the largest vegetated area in Area E at the beginning of the simulations, the total soil carbon stock of saltmarsh is also the largest in the site. The simulated living biomass carbon stock (above and below ground) of saltmarsh per area is $5.27 \text{ MgC} \cdot \text{ha}^{-1}$ and only accounts for 3% of the total carbon stock, as the soil carbon stock is $157 \text{ MgC} \cdot \text{ha}^{-1}$ (Table 1). In mangroves, the living biomass carbon stock per area represents 5% of the total carbon stock as the simulated living biomass carbon stock per area is $6.91 \text{ MgC} \cdot \text{ha}^{-1}$ and the soil carbon stock is $111 \text{ MgC} \cdot \text{ha}^{-1}$. These results are consistent with measured carbon content in newly colonized mangroves less than 15 years old (Kelleway et al., 2016) and saltmarsh areas in the region (Macreadie et al., 2017b), however, it must be noted that carbon in aboveground biomass of mature mangroves can reach values ten times higher than our simulated results (Kelleway et al., 2016; Serrano et al., 2019; Kauffman et al., 2020). Though we estimate rates of biomass production, our approach does not allow for accumulation of mangrove woody biomass, therefore, biomass carbon stocks are not calculated over time, only the contributions of belowground biomass to the soil carbon (C_{dr}). The total soil carbon stock of Area E amounts to 13300 MgC . We use this value as the initial soil carbon stock in the wetland.

Table 1. Simulated aboveground biomass for saltmarsh, simulated carbon stock in biomass and calculated soil carbon stock in Area E.

	Mangrove	Saltmarsh	Mudflat and tidal pools
Simulated aboveground biomass	($\text{Mg} \cdot \text{ha}^{-1}$)	($\text{Mg} \cdot \text{ha}^{-1}$)	
	8.09 ± 4.07	8.24 ± 1.37	
Carbon content	($\text{MgC} \cdot \text{ha}^{-1}$)	($\text{MgC} \cdot \text{ha}^{-1}$)	($\text{MgC} \cdot \text{ha}^{-1}$)
Aboveground biomass	3.80 ± 1.92	3.87 ± 0.64	
Belowground biomass	3.11 ± 1.35	1.40 ± 0.23	
Soil carbon (1m depth)	110.58 ± 35.53	156.55 ± 40.28	74.45 ± 22.69

Note: Values of average biomass, aboveground and belowground carbon in biomass represent the spatial average of simulated data.

3.2 Projections of biomass production and accretion

Figs. 3 and 4 show model results for the three scenarios in terms of vegetation distribution (Fig.3) and soil accretion (Fig.4). In the scenario with no-gate control, saltmarsh vegetation losses at the end of the simulation period are the most significant. Saltmarsh areas are able to cope with effects of sea-level rise for the first 40 years, but then there is a rapid decline due to submergence and mangrove encroachment, with a net loss of 40 ha of saltmarsh after 60 years (Figs. 3a and 4f). By the end of the simulation period, our results show a potential net loss of 60 ha of saltmarsh in the no-gate scenario (Figs. 3a and 4i). Conversely, mangroves are able to encroach on saltmarsh and establish in other locations of Area E which results in an increase of 20 ha of mangrove areas over the first 80 years of simulation; however, this gain in mangrove areas is lost after 100 years due to mangrove submergence (Figs. 3a and 4i). Despite saltmarsh areas showing a significant decrease in our simulations with no-gate control, the average productivity of aboveground biomass does not show a significant change over the simulation period, as the estimated saltmarsh aboveground biomass values are between $8.2 \text{ Mg} \cdot \text{ha}^{-1} \cdot \text{year}^{-1}$ to $9.6 \text{ Mg} \cdot \text{ha}^{-1} \cdot \text{year}^{-1}$ (Fig. 3d). Average accretion rates in saltmarsh areas increase from $1.3 \text{ mm} \cdot \text{year}^{-1}$ to $2.3 \text{ mm} \cdot \text{year}^{-1}$ over the first 80 years of simulation and decrease at the end of the simulation (Fig. 3g). For mangrove, despite an almost linear increase in area over the first 80 years with no-gate control (Fig. 3d,g), there is more variation in the average productivity of aboveground biomass and

average accretion rates than in saltmarsh. The initial average aboveground biomass productivity for mangrove is $8.1 \text{ Mg} \cdot \text{ha}^{-1} \cdot \text{year}^{-1}$, which decreases after 20 years when newly colonized mangrove establish in areas of lower D which leads to mangroves with lower biomass productivity (Fig. 3d). At the end of the simulation, there is an increase in the average aboveground mangrove biomass productivity, likely due to limited accommodation which precludes the establishment of newly colonized mangrove. The remaining mangrove areas have higher D values than in previous years, resulting in higher average aboveground biomass. Accretion rates in mangrove areas show a similar trend to the aboveground biomass. Initial average accretion rate for mangrove is $2.2 \text{ mm} \cdot \text{year}^{-1}$, which decreases to values between $1.2 \text{ mm} \cdot \text{year}^{-1}$ and $1.4 \text{ mm} \cdot \text{year}^{-1}$ between 20 and 80 years and increases at the end of the simulation period (Fig. 3g).

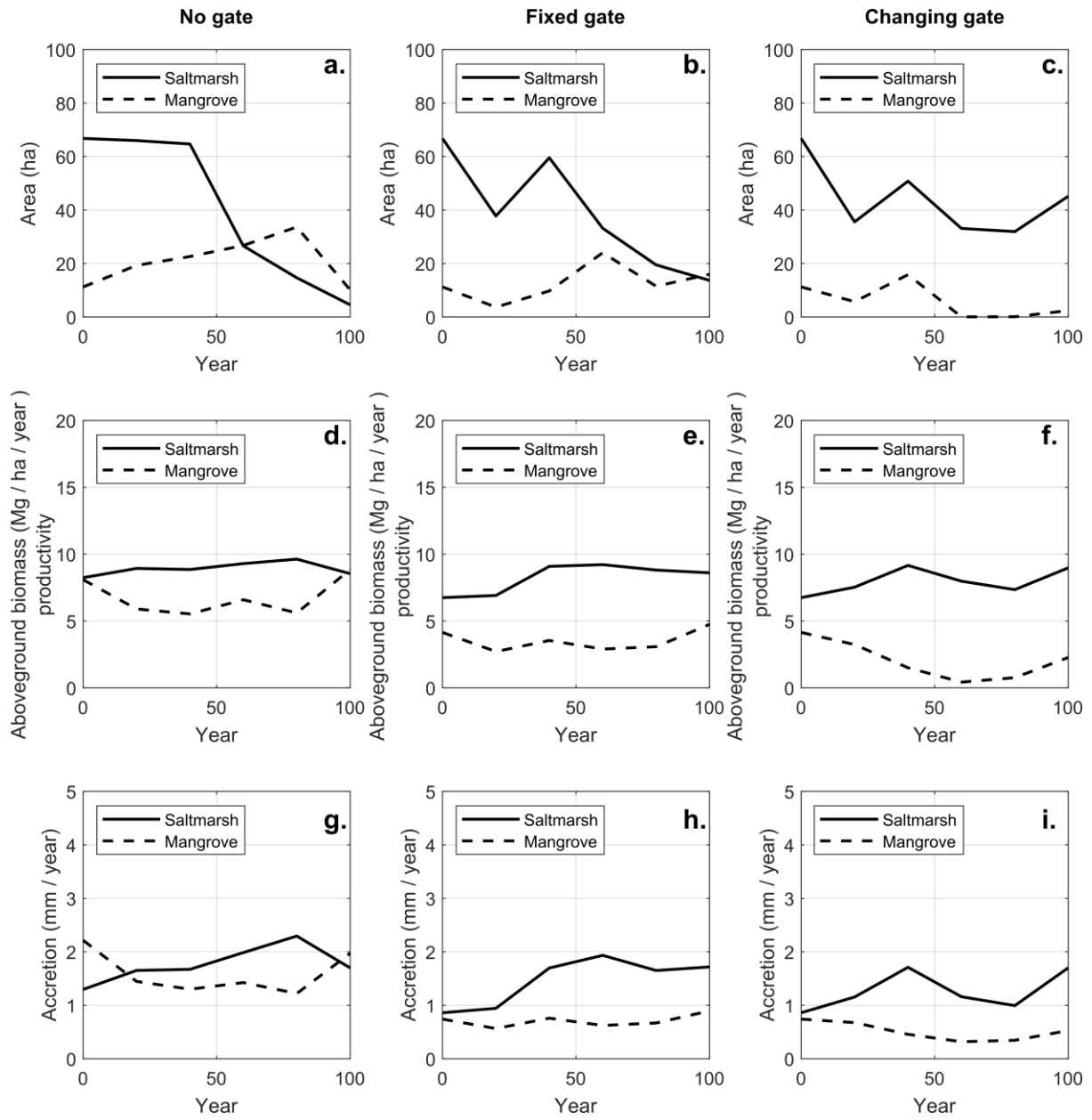


Figure 3. Simulated changes in vegetation extent in ha (a,b,c), aboveground biomass production in $\text{Mg} \cdot \text{ha}^{-1} \cdot \text{year}^{-1}$ (d,e,f), and accretion rates in $\text{mm} \cdot \text{year}^{-1}$ (g,h,i) under different control scenarios.

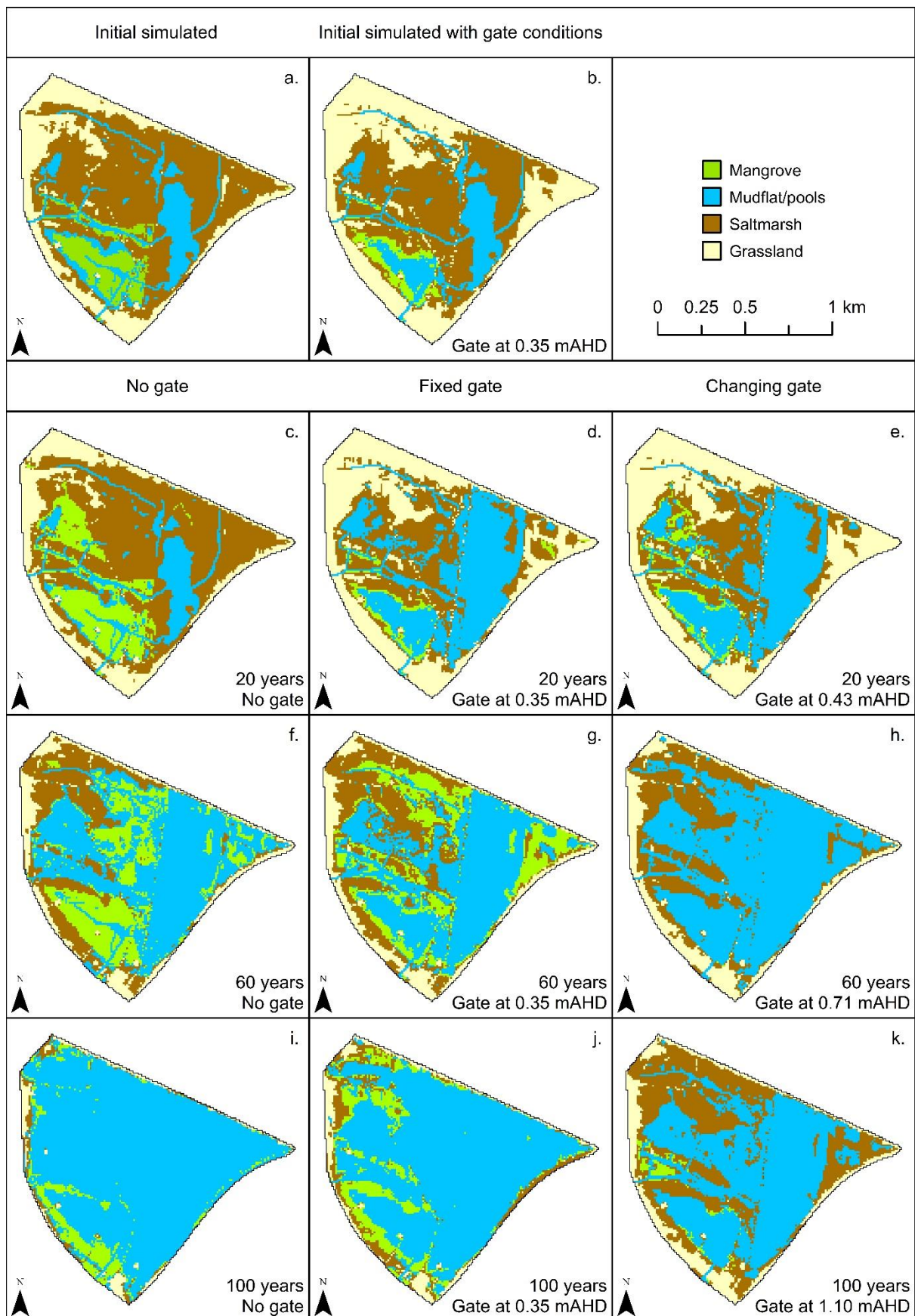


Figure 4. Changes in vegetation distribution. Simulated initial vegetation distribution with no gate control (a), and gate control (b). Simulated vegetation distribution after 20, 60 and 100

years with no-gate control (c,f,i), fixed gate control (d,g,j), and changing gate control (e,h,k). Note: Adapted from Sandi et al. (2018). Gate levels are presented in relationship to the current Australian Height Datum (AHD).

The inclusion of gate control in the wetland to limit mangrove encroachment on saltmarsh also promotes an initial decrease of saltmarsh in the upper areas of the wetland as a result of tidal attenuation. For our calculations of initial biomass productivity, initial accretion rates, and soil carbon sequestration with gate conditions, we used the estimated vegetation distribution just after the installation of the gate (Fig. 4b) which differs from the initial vegetation distribution without the gate (Fig. 4a). Our estimates show that after 20 years, gate control could potentially lead to a decrease in 30 ha of saltmarsh areas (Figs. 3b,c and 4d,e). In the scenario with fixed gate control, mangrove encroachment on saltmarsh is limited in the first 40 years, but eventually, mangrove encroaches on saltmarsh areas after 60 years and both mangrove and saltmarsh are submerged towards the end of the simulation period (Figs. 3e and 4g,j). During the first 20 years, average aboveground biomass production and average accretion rates in saltmarsh are lower in the scenario with fixed gate control than the scenario with no-gate, but after 40 years values are in a similar range ($8.6 - 9.2 \text{ Mg} \cdot \text{ha}^{-1} \cdot \text{year}^{-1}$ and $1.7 - 2.9 \text{ mm} \cdot \text{year}^{-1}$) (Fig. 3e,h). This suggests that as sea level rises the initial effects of hydraulic control from the fixed gate have less influence on the dynamics of the vegetation and accretion. In mangrove, areas variation of average aboveground biomass production and average accretion rates for the scenario with fixed gate control (Fig. 3e,h) have similar trends to the scenario with no-gate (Fig. 3d,g); however, magnitudes are around 50% lower than in the no-gate control scenario as the gate promotes the submergence of the mangrove in areas of high D early in the simulation and newly colonized mangrove is established in areas of low D , leading to lower biomass production and lower accretion rates (equations 1 and 2).

In the scenario with changing gate conditions, attenuation of the tidal regime promotes the establishment of saltmarsh areas at the end of the simulation period and the almost complete exclusion of mangroves after 60 years (Figs. 3c and 4h). Under the changing gate control scenario, hydraulic attenuation also produces lower average aboveground biomass production and average accretion rates in saltmarsh after 60 and 80 years, but increases at the end of the simulation (Fig. 3f,i). In mangroves, average aboveground biomass productivity decreases from the initial value of $8.1 \text{ Mg} \cdot \text{ha}^{-1} \cdot \text{year}^{-1}$ to $0.4 \text{ Mg} \cdot \text{ha}^{-1} \cdot \text{year}^{-1}$ and average accretion rates decrease from $0.7 \text{ mm} \cdot \text{year}^{-1}$ to $0.3 \text{ mm} \cdot \text{year}^{-1}$ after 60 years. Mangrove areas with changing gate conditions are very small after 60 years and do not significantly contribute to the vegetation dynamics of Area E (Figs. 3c and 4h,k).

3.3 Projection of soil carbon accumulation rates

Soil carbon accumulation rates show that higher rates per area occur under the no-gate control scenario for both saltmarsh and mangrove (Fig. 5a and 5g). For saltmarsh, our estimates show an initial average soil carbon accumulation rate per area of $1.0 \text{ MgC} \cdot \text{ha}^{-1} \cdot \text{year}^{-1}$ which increases to a maximum of $1.6 \text{ MgC} \cdot \text{ha}^{-1} \cdot \text{year}^{-1}$ after 80 years (Fig. 5a). In terms of the total soil carbon accumulation rates, initially, saltmarsh areas accumulate $70.6 \text{ MgC} \cdot \text{year}^{-1}$ which increases to $82.3 \text{ MgC} \cdot \text{year}^{-1}$ after 20 years and significantly reduces to $37.3 \text{ MgC} \cdot \text{year}^{-1}$ after 60 years and to $5.6 \text{ MgC} \cdot \text{year}^{-1}$ after 100 years (Figs. 5d and 6c,f,i). This decrease in the soil carbon accumulation rates occurs as saltmarsh is lost from submergence and mangrove encroachment (Fig. 4). The initial average soil carbon accumulation rate per area in mangroves is $1.0 \text{ MgC} \cdot \text{ha}^{-1} \cdot \text{year}^{-1}$ which decreases to $0.7 \text{ MgC} \cdot \text{ha}^{-1} \cdot \text{year}^{-1}$ after 20 years and remains low for most of the simulation period (Fig. 5g). The initial total soil carbon accumulation rate for mangrove is $11.0 \text{ MgC} \cdot \text{year}^{-1}$, which

reaches a maximum of $21.7 \text{ MgC} \cdot \text{year}^{-1}$ after 80 years and decreases to $10.0 \text{ MgC} \cdot \text{year}^{-1}$ after 100 years (Fig. 5j). The majority of the remaining vegetated areas at the end of the no-gate control simulation are mangrove areas (Fig. 4i), so in this scenario mangrove accounts for the majority of the soil carbon accumulation of the wetland after 100 years. However, by that point, the capacity for soil carbon sequestering of the site has reduced by 80% from the initial values given the vegetation loss (Fig. 4i and 6i).

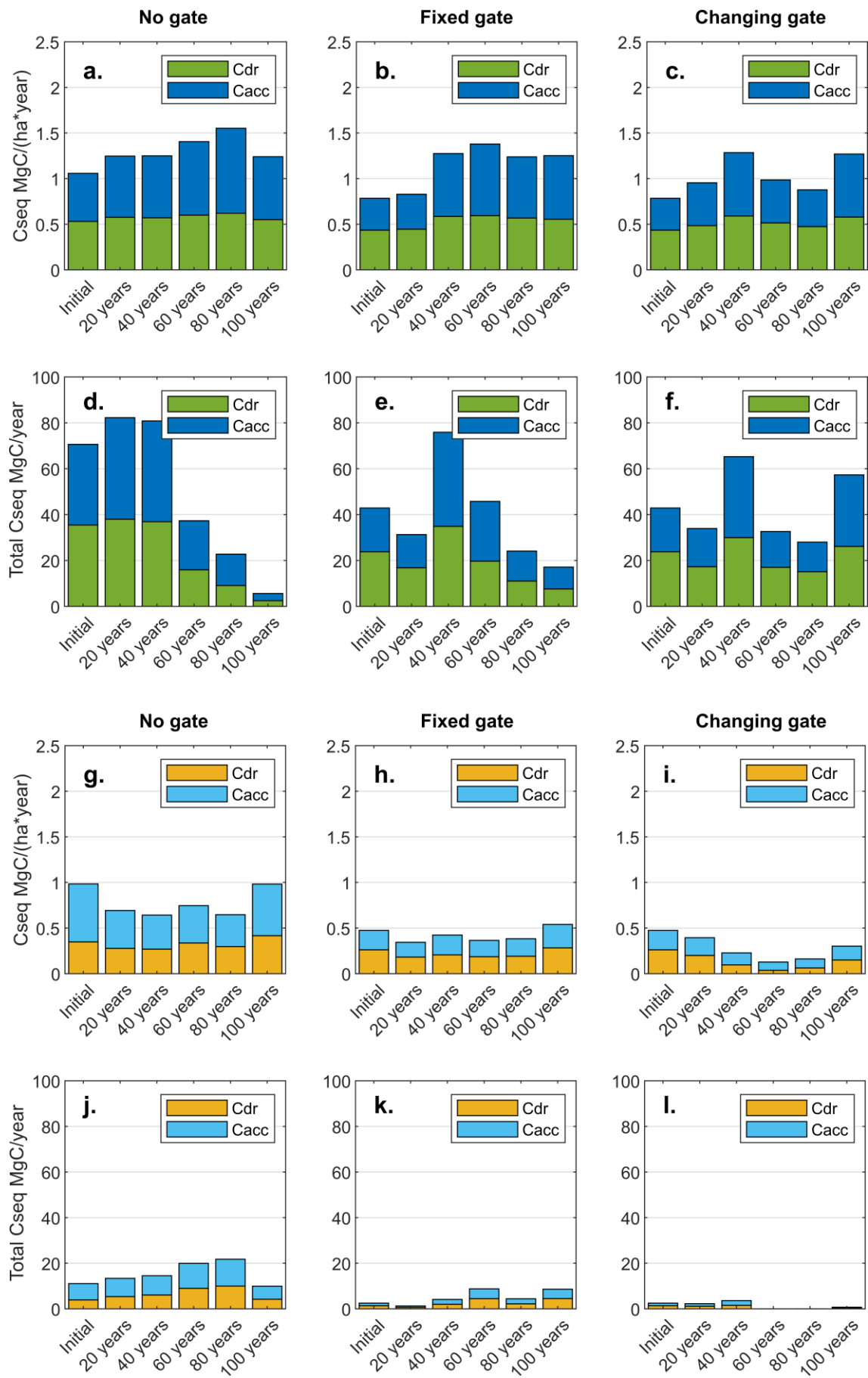


Figure 6. Average soil carbon sequestration rates per area ($\text{MgC} \cdot \text{ha}^{-1} \cdot \text{year}^{-1}$) from soil accretion (C_{acc}) and root decomposition (C_{dr}) for saltmarsh (a, b, c) , and otal carbon sequestration rates ($\text{MgC} \cdot \text{year}^{-1}$) for saltmarsh (d,e,f) under different management scenarios. Average carbon sequestration rates per area ($\text{MgC} \cdot \text{ha}^{-1} \cdot \text{year}^{-1}$) from soil accretion (C_{acc}) and root decomposition (C_{dr}) for mangrove (g,h,i), and total carbon sequestration rates ($\text{MgC} \cdot \text{year}^{-1}$) for mangrove (j,k,l) under different management scenarios.

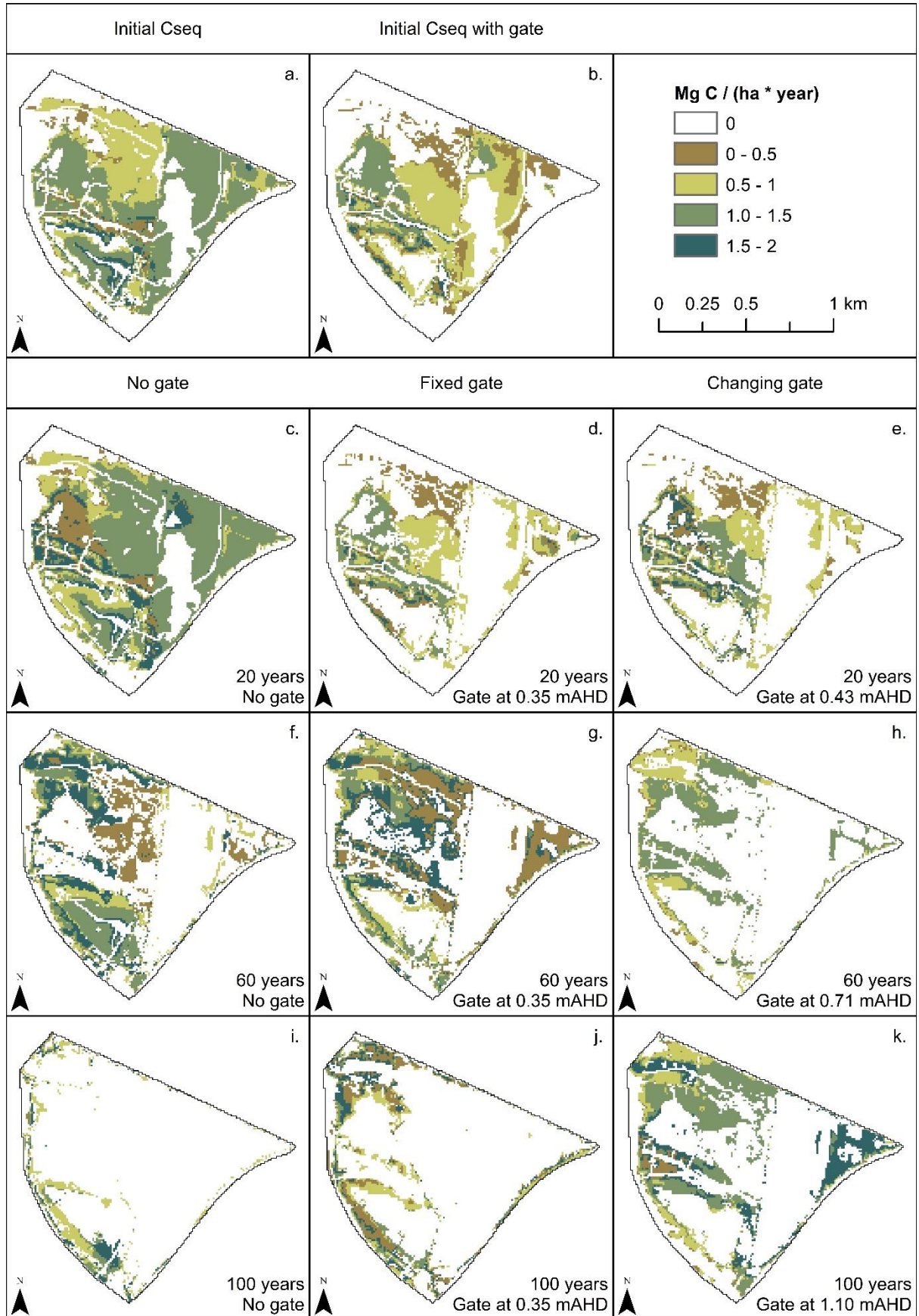


Figure 6. Changes in soil carbon accumulation rates per area ($\text{MgC} \cdot \text{ha}^{-1} \cdot \text{year}^{-1}$). Estimated initial carbon accumulation rates per area with no gate control (a), and gate control (b).

Simulated carbon accumulation rates per area after 20, 60 and 100 years with no-gate control (c,f,i), fixed gate control (d,g,j), and changing gate control (e,h,k). Gate levels are presented in relationship to the current Australian Height Datum (AHD).

In the scenarios with gate control, soil carbon accumulation rates per area are lower than in the no-gate control scenario as attenuation from hydraulic control limits both biomass productivity and accretion (Fig. 5b,c and 5h,i). The objective of the gate is to limit mangrove establishment, but also causes some initial saltmarsh area loss. With the introduction of the gate, the initial average soil carbon accumulation rate per area in saltmarsh is $0.8 \text{ MgC} \cdot \text{ha}^{-1} \cdot \text{year}^{-1}$ (Fig. 5b,c) and for mangrove is $0.5 \text{ MgC} \cdot \text{ha}^{-1} \cdot \text{year}^{-1}$ (Fig. 5h,i). The initial total soil carbon accumulation rate for saltmarsh decreases to $42.9 \text{ MgC} \cdot \text{year}^{-1}$ with the inclusion of the gate (Fig. 5e,f) and to $2.5 \text{ MgC} \cdot \text{year}^{-1}$ for mangrove (Fig. 5k,l). Soil carbon sequestered from mangrove is significant in the fixed control scenario after 60 years (Fig. 5k), when effects from the gate are less pronounced and newly colonized mangrove encroaches on saltmarsh. In the fixed gate scenario, soil carbon sequestered from mangrove areas contributes to more than 13% of the total sequestered soil carbon near the end of the simulation period (Fig. 5k). In the scenario with changing gate control, the total soil carbon sequestration from mangroves contributes to less than 5% of the sequestered soil carbon over the whole simulation period (Fig. 5l). At the end of the simulation, the combined total soil carbon accumulation rate of both mangrove and saltmarsh is of $15.6 \text{ MgC} \cdot \text{year}^{-1}$, $25.7 \text{ MgC} \cdot \text{year}^{-1}$ and $58.0 \text{ MgC} \cdot \text{year}^{-1}$ for the scenarios with no-gate, fixed gate and changing gate control respectively.

3.4 Changes in soil carbon stock

Sequestered soil carbon originating from soil carbon sequestration rates (Fig. 5) as well as potential carbon losses are converted to CO_2 to represent potential greenhouse gases burial and emissions on the study area for all scenarios (see section 2.4.4). Figure 7 shows the change in soil carbon stock (in MgC) as a result of cumulative CO_2 burial and CO_2 emissions (in MgCO_2). All control scenarios show steady rates of potential carbon loss (CO_2 emissions) that are much lower than the sequestered soil carbon (CO_2 burial) resulting in a net increase of carbon stock (in MgC) over the years (Fig 7). In the scenario with no-gate control, CO_2 burial rate decreases after 60 years, when saltmarsh vegetation is significantly lost due to submergence and mangrove encroachment occurs (Fig. 7a). The total soil carbon stock in the site reaches approximately 20800 MgC after 100 years under no-gate conditions, with a net soil carbon gain of 56% of the initial stock. In the scenarios with gate control, submergence and transition to grassland occurs early in the simulations due to the effects of the gate, which reduces the capacity for CO_2 burial (Fig. 7a). The total soil carbon stocks reach values of 18100 MgC and 17500 MgC under the fixed gate and changing gate control scenarios respectively (Fig. 7c). These correspond to net soil carbon gains of 36% and 32% at the end of the simulation period, around 20% less than the scenario with no-gate control. Both gated scenarios have the same dynamics of soil carbon stock.

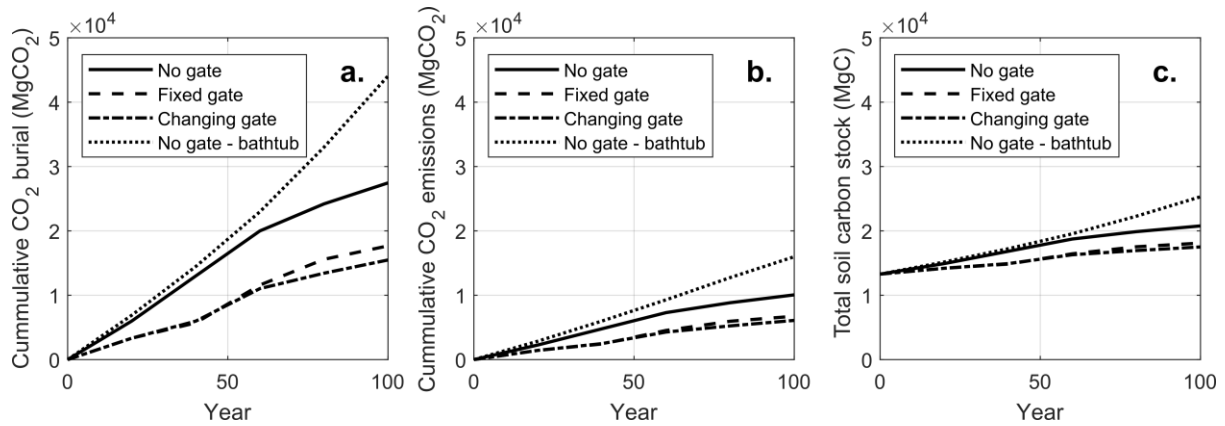


Figure 7. Soil carbon dynamics in Area E under different control scenarios. Cumulative CO₂ burial (a), CO₂ emissions (b), and total soil carbon stock (c).

For comparison, we also estimated soil carbon burial and carbon emissions using a simpler bathtub approach. In the bathtub model simulation, mangrove vegetation encroaches on saltmarsh very early in the simulation, there is little vegetation submergence at the end of the simulation period and accretion rates are much higher than the hydrodynamic model simulations (Supplementary Figure 6). The trends of cumulative CO₂ burial and CO₂ emissions are similar over the first 60 years of simulation, but by using the bathtub approach, the estimated cumulative CO₂ burial is grossly over predicted at the end of the simulation (Fig. 7a), resulting in a total soil carbon stock of approximately 25300 MgC after 100 years (Fig. 7c), which is 1.2 times the values expected using the hydrodynamic approach. Cumulative CO₂ emissions also show higher magnitudes using the bathtub approach at the end of the simulation. After 60 years of simulation, soil carbon burial and emissions are less in the hydrodynamic model than the bathtub model because most vegetation drowns.

4 Discussion

Soil carbon sequestration in estuarine and coastal wetlands produces some of the most carbon-rich soils in the world. Knowledge of the previous conditions, as well as analysis of the historic environmental processes, are important when estimating soil carbon budgets because the variations of the carbon along the soil profile are the result of different environmental conditions over time (Kelleway et al., 2017a). In our study area, the majority of the area was covered by saltmarsh since before the 1950s (Williams et al., 2000), but mangroves only established at the site after tidal flows were reinstated during the 1990s (Howe et al., 2010). Because of this, the saltmarsh at the site is well established while mangroves are relatively less mature. Our estimate of the soil carbon stock in saltmarsh (157 MgC·ha⁻¹) is consistent with estimates of soil carbon stocks in Australian saltmarshes (165 MgC·ha⁻¹) estimated by Macreadie et al. (2017b) and (168 MgC·ha⁻¹) estimated by Serrano et al. (2019). Our estimate of the soil carbon stock for mangroves (111 MgC·ha⁻¹) reflects the age since establishment as it is lower than estimates of mangrove soil carbon stocks collated by (Serrano et al., 2019) for Australian mangroves (251 MgC·ha⁻¹). Estimates soil carbon stocks for Australian mangroves are generally lower than other estimates in the Indo Pacific region (783 MgC·ha⁻¹ on average) (Donato et al., 2011); however, the data reported by Donato et al. (2011) includes a wide range of mangrove species, soils (ranging from <0.5 m to deep >3 m), and the environmental history was not taken into account. Our estimate of the soil carbon stock in mangroves is consistent with belowground soil carbon stocks reported for

mangroves between 0 - 15 years of age (Kelleway et al., 2016), which is roughly the age of the mangroves at the site at the initial time of the simulations.

Our estimated initial average soil carbon sequestration rate per area (C_{seq}) for saltmarsh is $1.0 \text{ MgC}\cdot\text{ha}^{-1}\cdot\text{year}^{-1}$, which is in between values reported by Serrano et al. (2019) ($0.39 \text{ MgC}\cdot\text{ha}^{-1}\cdot\text{year}^{-1}$), Macreadie et al. (2017b) ($0.55 \text{ MgC}\cdot\text{ha}^{-1}\cdot\text{year}^{-1}$) and Ouyang and Lee (2014) ($2.75 \text{ MgC}\cdot\text{ha}^{-1}\cdot\text{year}^{-1}$) for Australian saltmarshes, and lower than global values reported for saltmarsh ($1.51 \text{ MgC}\cdot\text{ha}^{-1}\cdot\text{year}^{-1}$) (Duarte et al., 2005). In our calculations, half of the saltmarsh carbon accumulation rates originate from soil accretion (Fig. 5a), which results in $0.5 \text{ MgC}\cdot\text{ha}^{-1}\cdot\text{year}^{-1}$, very close to the value of soil carbon accumulation rate reported by Macreadie et al. (2017b). The remaining half of the soil carbon accumulation rate in our calculations originates from dead root turnover (Fig. 5a), which was not included by Macreadie et al. (2017b) or Serrano et al. (2019). For mangrove, our estimate of the initial average soil carbon sequestration rate per area (C_{seq}) is $1.0 \text{ MgC}\cdot\text{ha}^{-1}\cdot\text{year}^{-1}$ which is lower than values reported by Saintilan et al. (2013) ($2.56 \text{ MgC}\cdot\text{ha}^{-1}\cdot\text{year}^{-1}$), Serrano et al. (2019) ($1.26 \text{ MgC}\cdot\text{ha}^{-1}\cdot\text{year}^{-1}$), and above the mean value reported by Lovelock et al. (2014) ($0.76 \text{ MgC}\cdot\text{ha}^{-1}\cdot\text{year}^{-1}$). For mangrove, one-third of the soil carbon accumulation rates originates from dead root turnover and the remaining two-thirds are the result of accretion (Fig. 5g). Lovelock et al. (2014) argued that their low rates of soil carbon sequestration in mangroves may be related to the exclusion of the contribution from roots throughout the soil profile in their estimates. Our estimates of soil carbon accumulation rates integrate turnover from dead roots as part of the calculations as opposed to only increases of the top-soil layer. Lamont et al. (2020) suggest substantial carbon sequestration in deeper soils originating from dead roots turnover.

Analysis of the model results for the three scenarios of management via tidal inlet control reflects the strong influence of flow conditions on the vegetation distribution and extent and the resulting aboveground biomass production. Scenarios with tidal regimes affected by gate control show an overall initial decrease in aboveground biomass production and changes in the spatial distribution of saltmarsh vegetation compared to the no-gate scenario due to increased hydrodynamic attenuation. Consequently, different spatial changes on the soil carbon accumulation rates occur across the site and over time for different scenarios (Fig. 6). In the scenario with no-gate control saltmarsh is rapidly displaced by mangrove encroachment, reducing its soil carbon accumulation rates. In the gate-controlled scenarios, the initial soil carbon accumulation rates for saltmarsh are lower than in the no-gate scenario due to the reduced inundation levels, and continue to be lower for the first 40 years of simulation (Fig. 5). In the changing gate scenario, mangrove establishment is limited and saltmarsh vegetation is promoted at the end of the simulation, resulting in an increase in soil carbon accumulation rates. Under no-gate scenario, the initial mangrove areas at the lower end of the tidal frame remain for most of the simulation period reaching mature age (Fig. 4), but they become submerged at the end of the simulation period. As sea-level rise occurs, mangroves can colonize new areas with low D , which translates into newly colonized mangroves with lower biomass production rates, but still capable of sequestering considerable soil carbon via root decomposition (C_{dr}) (Fig. 5). With the inclusion of the inlet control gate, the initial mangrove areas completely disappear (due to drowning) early in the simulation (Fig. 4), resulting in less initial capacity to sequester soil carbon (Figs. 5) and also in a reduction of future capacity as those mangrove areas do not reach a mature age. In the fixed gate scenario, newly colonized mangroves with lower biomass get established in other areas of the wetland as sea level rises, but the mangrove spatial distribution changes frequently (Fig. 4) resulting in ephemeral wetland areas due to short-term establishment and die-off of mangroves. This is also reflected in the results showing less soil carbon





accumulation rates in the fixed gate control scenario than the scenario with no-gate (Fig. 5). In the changing gate scenario mangrove establishment is limited for all the simulation period, so only saltmarsh contributes to soil carbon sequestration. Importantly, our model does not only simulate the spatial distribution of the vegetation, but also provides estimates of carbon accumulation rates that are spatially varied and consistent with expected vegetation structures and age.

Previous estimates of the effects sea-level rise on the soil carbon sequestration of saltmarsh environments suggest that carbon burial might increase in the first half of the century, followed by a decrease towards the end of the century (Kirwan & Mudd, 2012). This is consistent with our findings as there is a decrease in the rate of CO₂ burial (Fig. 7a) and a decrease in the capacity of the wetland for soil carbon accumulation under no-gate control (Figs. 5d and 5j), mostly as a result of vegetation submergence after 60 years, but also due to the fact that new vegetation areas have less biomass productivity and less capacity for soil carbon accumulation from accretion and dead root turnover. Though current projections of sea-level rise show continuous increases in sea-level rise rates over the next century, historical records show that these rates have varied over different time-scales, indicating more rapid acceleration in some decades and less rapid acceleration in others. Over millennia, global trends of sea-level rise have also accelerated and decelerated, leading to coastal wetland retreat and expansion. Analysis of paleo-records linking sea-level rise rates with capacity of vegetation to initiate accretion show widespread submergence occurs in coastal wetlands when sea-level rise rates surpass 7 mm/year (Horton et al., 2018; Törnqvist et al., 2020; Saintilan et al., 2020). In our simulations, this rate of sea-level rise occurs after 60 years when the widespread loss of vegetation is likely to occur. Landward colonization and further accommodation in the study site is not possible due to the embankments surrounding it. This accommodation might alleviate the significant reduction in carbon accumulation rates induced by vegetation submergence (Lovelock & Reef, 2020); however, topography and anthropogenic barriers commonly limit accommodation in many other sites and regions. In the cases where vegetation could be able to colonize landwards, the wetland might also be unable to adapt vertically if accelerated sea-level rise continues and surpasses the 7 mm/year threshold derived from paleo-records. Under more attenuated conditions (scenarios with gate control), the capacity of the study area for CO₂ burial decreases (Fig. 7), but the wetland has higher rates of soil carbon accumulation at the end of the simulation period (Fig. 6j,k) as more vegetation is able to survive. Despite these higher rates, the final soil carbon stocks are significantly lower than in the no-gate scenario (Fig. 7c) and the newly established vegetation might not be able to adapt if accelerated sea-level rise continues beyond the period of analysis.

Due to the complex eco-geomorphic interactions between water, sediments and vegetation, the planning of coastal wetland rehabilitation and wetland creation should incorporate detailed modelling under sea-level rise and management scenarios. In our simulations, we have included three simplistic hydraulic control conditions and we found that there is a trade-off between strategies that guarantee the survival of the wetland and the total soil carbon sequestered. In the no-gate control scenario, the wetland was able to sequester more soil carbon by the end of the simulation than in the gate-controlled scenarios even when high emissions occurred following vegetation submergence (Table 2). In the gate-controlled scenarios, the presence of more vegetation than for the no-gate scenario leads to more habitat provision towards the end of the simulation; however, the newly colonized vegetation has lower aboveground biomass productivity due to the restrictions to the tidal regime and hydraulic attenuation and therefore there is less total soil carbon gains in the gate-controlled scenarios (Table 2). The scenario with changing-gate control has the highest soil carbon

sequestering capacity at the end of the simulation period, but it has the lowest soil carbon gains of the three management scenarios (Table 2). These results have significant implications for the management of coastal wetlands. Currently, coastal wetland accounting, wetland creation, wetland rehabilitation and wetland protection frameworks have identified the significance of wetland conservation for emission reduction programs such as REDD+ (Adame et al., 2018; Rogers et al., 2019a; Cameron et al., 2019). Rehabilitated wetlands have shown great capacity to sequester soil carbon at rates similar or higher than those of natural wetlands (Cameron et al., 2019) and created wetlands seem to be able to cope with the effects of sea-level rise under current conditions and the more conservative emissions scenarios (Krauss et al., 2017). However, predictions under future sea-level rise rely on assumptions of soil carbon sequestration capacity remaining at current levels and simplified inundation formulations that do not account for local wetland features. These assumptions are particularly restrictive for predictions using scenarios of high CO₂ emissions and accelerated sea-level rise, in which important changes to the wetland vegetation structure and spatial distribution are predicted to occur faster than for any contemporary observational period. Therefore, implementation of a detailed modelling framework like the one developed here and projections of vegetation changes and soil carbon sequestration under sea-level rise can help evaluating management strategies to obtain the best outcomes for habitat provision and soil carbon sequestration.

Table 2. Trade-off between wetland vegetation loss and soil carbon stock gains.

Control	Percent wetland survival (%)		Percent increase in soil carbon stock (%)	
No Gate	 More habitat loss	19	 More carbon gain	56
Fixed Gate		38		36
Rising Gate		61		32
		 Less habitat loss		 Less carbon gains

Other effects of climate change on vegetation and soil carbon dynamics are less obvious and harder to integrate into modelling frameworks. For example, increased temperature and drought effects can lead to increased forest mortality, but higher CO₂ concentrations can alleviate some of these effects through CO₂ fertilization (Liu et al., 2017). Furthermore, in mangrove-saltmarsh wetlands increased CO₂ may affect competition between mangrove (C₃ photosynthetic path) and saltmarsh (C₃ and C₄ photosynthetic path) species (McKee & Rooth, 2008; Howard et al., 2018). Mangrove encroachment on saltmarsh might decline due to increased resource competition (McKee & Rooth, 2008) as salinity can be a larger driver for mangrove encroachment than increases in CO₂ (Reef et al., 2015; Ball et al., 1997). In turn, saltmarsh C₃ species have been reported to have a larger increase in biomass in response to CO₂ fertilization than C₄ saltmarsh species (Arp et al., 1993), although Ratliff et al. (2015) did not find the differences to be significant. As the saltmarsh species in our study area are both C₃ (*Sarcocornia quinqueflora*) and C₄ (*Sporobolus virginicus*) it is possible that increased CO₂ may favour a shift to *Sarcocornia* dominance, and an increase on saltmarsh biomass productivity and accretion capacity. This suggests that effects of increased CO₂ in the atmosphere might contribute to more soil carbon burial from saltmarsh than what

our estimates indicate. The magnitude of the increase in soil carbon burial is uncertain, as biomass productivity increase due to CO₂ fertilization estimates vary widely and maybe limited by nitrogen availability (Ratliff et al., 2015). Additionally, it must be noted that saltmarsh and mangroves occur along a continuum from sediment-rich to sediment-poor environments, where organic soil contribution from plants has a major role in the accretion and survival of the latter (Cahoon et al., 2020). Because of this, accretion, survival and soil carbon sequestration capacity in mangrove-saltmarsh wetlands that receive considerable amounts of sediment may not benefit as much from biomass productivity increases, but there could be significant benefits for sediment-poor wetlands.

Findings presented here show detailed calculation of different processes contributing to soil carbon accumulation. Dynamics of total carbon budgets, however, must include blue carbon stored in aboveground and belowground biomass stocks which our eco-geomorphic approach does not provide. Even though in our case most of the carbon is stored in the soil (95%), carbon stored in aboveground biomass can be a significant fraction of the total carbon stock, in particular for mangroves. For example, in *Avicennia spp.*, this fraction can be up to 25% of the total carbon budget considering the top 1m layer of the soil (Kauffman et al., 2020). In Australian ecosystems, mangrove aboveground biomass carbon is around 20% of the total carbon budget in temperate and subtropical climate regions and up to 44% in tropical climates (Serrano et al., 2019). In our approach, we focus on the soil carbon and use calculations of aboveground biomass productivity in terms of the inundation descriptor D (equation 2), for both saltmarsh and mangroves, each with their respective calibrated parameters. More complex relationships can be developed based on formulations for individual mangrove tree growth (van Maanen et al., 2015; Chen & Twilley, 1998), but they require the definition of a larger number of parameters than equation 2.

5 Summary and conclusions

Although blue carbon ecosystems have been the focus of several research in recent years, the impacts of accelerated sea-level rise on the future of coastal wetlands, particularly their capacity for soil carbon accumulation remains uncertain. Current understanding of coastal wetland processes suggests that future tidal reinstatement, wetland restoration and landward colonization induced by sea-level rise present an opportunity for potential gains of soil carbon. However, estimates of the magnitude of future soil carbon gains often rely on assumptions of sequestration capacity remaining at current levels, uniform wetland inundation levels (i.e., bathtub approach), and availability of upland areas for wetland transgression into existing less productive ecosystems.

Our results, using an eco-geomorphic model that includes soil carbon processes, show that under accelerated sea-level rise the combined effects of rapid vegetation retreat and colonization affected by local wetland features produces a shift to newly colonized vegetation that have lower capacity for soil carbon accumulation. Results using the model with uniform wetland inundation levels (bathtub) grossly over predicts (by 60%) the accumulated soil carbon burial at the end of the 100-yr simulation period.

Our baseline scenario, assuming no inlet control post wetland restoration, shows the highest total soil carbon accumulated at the end of the simulation period, but also the highest decrease in soil carbon accumulation capacity with respect to initial values due to vegetation submergence and resulting newly colonized vegetation. In the other two scenarios, inlet control (a common management strategy) is used to manage sea-level rise effects and conserve vegetation and bird habitat, but early disappearance of mature mangrove vegetation and establishment of newly colonized vegetation decreases soil carbon accumulation rates

which results in 20% less of the soil carbon sequestered in the baseline scenario. The capacity for soil carbon accumulation at the end of the simulation is higher in the controlled scenarios as more vegetated areas survive submergence, but it is likely that this capacity will decrease if accelerated sea-level rise continues.

These results highlight the importance of implementing an eco-geomorphic modelling framework to study the dynamics of soil carbon in coastal wetlands. The implementation of management strategies needs to not only aim at preserving wetland areas and habitat, but also to provide conditions to preserve vegetation with significant capacity for soil carbon accumulation.

Acknowledgments

P.S. acknowledges support from the Australian Research Council (grant DP140104178 and Future Fellowship grant FT140100610).

Author contributions: **Steven G. Sandi:** Conceptualization, Investigation, Methodology, Visualization and Writing-Original draft. **Jose. F Rodriguez:** Conceptualization, Methodology, Supervision and Writing-Review & Editing. **Patricia M. Saco:** Conceptualization, Methodology Supervision and Writing-Review & Editing. **Neil Saintilan:** Conceptualization and Writing-Review & Editing. **Gerardo Riccardi:** Methodology and Writing-Review & Editing.

Data availability

Full description of the carbon model parameters has been provided in text and supporting information. This research uses hydrodynamic and vegetation simulation data from a previously developed model by Rodríguez et al. (2017) and Sandi et al. (2018). These data have been made available at <https://doi.org/10.4211/hs.db2cc5d068c04a2da47496c7265d3025>

References

- Donato, D. C., Kauffman, J. B., Murdiyarso, D., Kurnianto, S., Stidham, M., & Kanninen, M. (2011). Mangroves among the most carbon-rich forests in the tropics. *Nature Geoscience*, 4(5), 293-297. 10.1038/ngeo1123. <http://dx.doi.org/10.1038/ngeo1123>
- Ouyang, X., & Lee, S. Y. (2014). Updated estimates of carbon accumulation rates in coastal marsh sediments. *Biogeosciences*, 11(18), 5057-5071. <https://www.biogeosciences.net/11/5057/2014/>
- Howard, J., Hoyt, S., Isensee, K., Telszewski, M., & Pidgeon, E. (2014). *Coastal blue carbon: methods for assessing carbon stocks and emissions factors in mangroves, tidal salt marshes, and seagrasses*. Retrieved from Arlington, Virginia, USA.:
- Lovelock, C. E., Ruess, R. W., & Feller, I. C. (2011). CO₂ Efflux from Cleared Mangrove Peat. *PLOS ONE*, 6(6), e21279. <https://doi.org/10.1371/journal.pone.0021279>
- Pendleton, L., Donato, D. C., Murray, B. C., Crooks, S., Jenkins, W. A., Sifleet, S., Craft, C., Fourqurean, J. W., et al. (2012). Estimating Global “Blue Carbon” Emissions from Conversion and Degradation of Vegetated Coastal Ecosystems. *PLOS ONE*, 7(9), e43542. <https://doi.org/10.1371/journal.pone.0043542>
- Atwood, T. B., Connolly, R. M., Almahasheer, H., Carnell, P. E., Duarte, C. M., Ewers Lewis, C. J., Irigoien, X., Kelleway, J. J., et al. (2017). Global patterns in mangrove soil carbon stocks and losses. *Nature Clim. Change*, 7(7), 523-528. Article. <http://dx.doi.org/10.1038/nclimate3326>
- Lovelock, C. E., Atwood, T., Baldock, J., Duarte, C. M., Hickey, S., Lavery, P. S., Masque, P., Macreadie, P. I., et al. (2017). Assessing the risk of carbon dioxide emissions from blue carbon ecosystems. *Frontiers in Ecology and the Environment*, 15(5), 257-265. <https://esajournals.onlinelibrary.wiley.com/doi/abs/10.1002/fee.1491>

- Macreadie, P. I., Nielsen, D. A., Kelleway, J. J., Atwood, T. B., Seymour, J. R., Petrou, K., Connolly, R. M., Thomson, A. C. G., et al. (2017a). Can we manage coastal ecosystems to sequester more blue carbon? *Frontiers in Ecology and the Environment*, 15(4), 206-213. <http://dx.doi.org/10.1002/fee.1484>
- Adame, M. F., Najera, E., Lovelock, C. E., & Brown, C. J. (2018). Avoided emissions and conservation of scrub mangroves: potential for a Blue Carbon project in the Gulf of California, Mexico. *Biology Letters*, 14(12), 20180400.
- Rogers, K., Macreadie, P. I., Kelleway, J. J., & Saintilan, N. (2019a). Blue carbon in coastal landscapes: a spatial framework for assessment of stocks and additionality. *Sustainability Science*, 14(2), 453-467. <https://doi.org/10.1007/s11625-018-0575-0>
- Thorhaug, A. L., Poulos, H. M., López-Portillo, J., Barr, J., Lara-Domínguez, A. L., Ku, T. C., & Berlyn, G. P. (2019). Gulf of Mexico estuarine blue carbon stock, extent and flux: Mangroves, marshes, and seagrasses: A North American hotspot. *Science of The Total Environment*, 653, 1253-1261. <http://www.sciencedirect.com/science/article/pii/S0048969718338816>
- Macreadie, P. I., Ollivier, Q. R., Kelleway, J. J., Serrano, O., Carnell, P. E., Ewers Lewis, C. J., Atwood, T. B., Sanderman, J., et al. (2017b). Carbon sequestration by Australian tidal marshes. *Scientific Reports*, 7(1), 44071. <https://doi.org/10.1038/srep44071>
- Roner, M., D'Alpaos, A., Ghinassi, M., Marani, M., Silvestri, S., Franceschinis, E., & Realdon, N. (2016). Spatial variation of salt-marsh organic and inorganic deposition and organic carbon accumulation: Inferences from the Venice lagoon, Italy. *Advances in Water Resources*, 93, 276-287. <http://www.sciencedirect.com/science/article/pii/S0309170815002705>
- Morris, J. T., Barber, D. C., Callaway, J. C., Chambers, R., Hagen, S. C., Hopkinson, C. S., Johnson, B. J., Megonigal, P., et al. (2016). Contributions of organic and inorganic matter to sediment volume and accretion in tidal wetlands at steady state. *Earth's Future*, 4(4), 110-121. <https://agupubs.onlinelibrary.wiley.com/doi/abs/10.1002/2015EF000334>
- Ouyang, X., Lee, S. Y., & Connolly, R. M. (2017). The role of root decomposition in global mangrove and saltmarsh carbon budgets. *Earth-Science Reviews*, 166, 53-63. <http://www.sciencedirect.com/science/article/pii/S0012825216301258>
- Kelleway, J. J., Saintilan, N., Macreadie, P. I., Baldock, J. A., Heijnis, H., Zawadzki, A., Gadd, P., Jacobsen, G., et al. (2017a). Geochemical analyses reveal the importance of environmental history for blue carbon sequestration. *Journal of Geophysical Research: Biogeosciences*, 122(7), 1789-1805. <https://agupubs.onlinelibrary.wiley.com/doi/abs/10.1002/2017JG003775>
- Pérez, A., Libardoni, B. G., & Sanders, C. J. (2018). Factors influencing organic carbon accumulation in mangrove ecosystems. *Biology Letters*, 14(10), 20180237. <https://royalsocietypublishing.org/doi/abs/10.1098/rsbl.2018.0237>
- Kusumaningtyas, M. A., Hutahaean, A. A., Fischer, H. W., Pérez-Mayo, M., Ransby, D., & Jennerjahn, T. C. (2019). Variability in the organic carbon stocks, sources, and accumulation rates of Indonesian mangrove ecosystems. *Estuarine, Coastal and Shelf Science*, 218, 310-323. <http://www.sciencedirect.com/science/article/pii/S0272771418304207>
- Abbott, K. M., Elsey-Quirk, T., & DeLaune, R. D. (2019). Factors influencing blue carbon accumulation across a 32-year chronosequence of created coastal marshes. *Ecosphere*, 10(8), e02828. <https://esajournals.onlinelibrary.wiley.com/doi/abs/10.1002/ecs2.2828>
- Rogers, K., Kelleway, J. J., Saintilan, N., Megonigal, J. P., Adams, J. B., Holmquist, J. R., Lu, M., Schile-Beers, L., et al. (2019b). Wetland carbon storage controlled by millennial-scale variation in relative sea-level rise. *Nature*, 567(7746), 91-95. <https://doi.org/10.1038/s41586-019-0951-7>
- Watanabe, K., Seike, K., Kajihara, R., Montani, S., & Kuwae, T. (2019). Relative sea-level change regulates organic carbon accumulation in coastal habitats. *Global Change Biology*, 25(3), 1063-1077. <https://onlinelibrary.wiley.com/doi/abs/10.1111/gcb.14558>
- Breithaupt, J. L., Smoak, J. M., Bianchi, T. S., Vaughn, D. R., Sanders, C. J., Radabaugh, K. R., Osland, M. J., Feher, L. C., et al. (2020). Increasing Rates of Carbon Burial in Southwest Florida Coastal Wetlands. *Journal of Geophysical Research: Biogeosciences*, 125(2), e2019JG005349. <https://agupubs.onlinelibrary.wiley.com/doi/abs/10.1029/2019JG005349>
- Krauss, K. W., Cormier, N., Osland, M. J., Kirwan, M. L., Stagg, C. L., Nestlerode, J. A., Russell, M. J., From, A. S., et al. (2017). Created mangrove wetlands store belowground carbon and surface elevation change enables them to adjust to sea-level rise. *Scientific Reports*, 7(1), 1030. <https://doi.org/10.1038/s41598-017-01224-2>
- Wang, F., Lu, X., Sanders, C. J., & Tang, J. (2019). Tidal wetland resilience to sea level rise increases their carbon sequestration capacity in United States. *Nature Communications*, 10(1), 5434. <https://doi.org/10.1038/s41467-019-13294-z>
- Kirwan, M. L., & Mudd, S. M. (2012). Response of salt-marsh carbon accumulation to climate change. *Nature*, 489, 550. <http://dx.doi.org/10.1038/nature11440>

- Lovelock, C. E., & Reef, R. (2020). Variable Impacts of Climate Change on Blue Carbon. *One Earth*, 3(2), 195-211. <http://www.sciencedirect.com/science/article/pii/S2590332220303547>
- Kirwan, M. L., & Megonigal, J. P. (2013). Tidal wetland stability in the face of human impacts and sea-level rise. *Nature*, 504(7478), 53-60. Insight. <http://dx.doi.org/10.1038/nature12856>
- Kirwan, M. L., Temmerman, S., Skeehean, E. E., Guntenspergen, G. R., & Fagherazzi, S. (2016). Overestimation of marsh vulnerability to sea level rise. *Nature Climate Change*, 6(3), 253-260.
- Saco, P. M., & Rodríguez, J. F. (2013). 2.14 Modeling Ecogeomorphic Systems. In J. F. Shroder (Ed.), *Treatise on Geomorphology* (pp. 201-220). San Diego: Academic Press.
- Passeri, D. L., Hagen, S. C., Medeiros, S. C., Bilskie, M. V., Alizad, K., & Wang, D. (2015). The dynamic effects of sea level rise on low-gradient coastal landscapes: A review. *Earth's Future*, 3(6), 159-181. <http://dx.doi.org/10.1002/2015EF000298>
- Lentz, E. E., Thieler, E. R., Plant, N. G., Stippa, S. R., Horton, R. M., & Gesch, D. B. (2016). Evaluation of dynamic coastal response to sea-level rise modifies inundation likelihood. *Nature Clim. Change*, 6(7), 696-700. Letter. <http://dx.doi.org/10.1038/nclimate2957>
- Alizad, K., Hagen, S. C., Morris, J. T., Bacopoulos, P., Bilskie, M. V., Weishampel, J. F., & Medeiros, S. C. (2016a). A coupled, two-dimensional hydrodynamic-marsh model with biological feedback. *Ecological Modelling*, 327(Supplement C), 29-43. <http://www.sciencedirect.com/science/article/pii/S0304380016300011>
- Rodríguez, J. F., Saco, P. M., Sandi, S., Saintilan, N., & Riccardi, G. (2017). Potential increase in coastal wetland vulnerability to sea-level rise suggested by considering hydrodynamic attenuation effects. *Nature Communications*, 8, 16094. Article. <http://dx.doi.org/10.1038/ncomms16094>
- Kelleway, J. J., Saintilan, N., Macreadie, P. I., Skilbeck, C. G., Zawadzki, A., & Ralph, P. J. (2016). Seventy years of continuous encroachment substantially increases 'blue carbon' capacity as mangroves replace intertidal salt marshes. *Global Change Biology*, 22(3), 1097-1109. <http://dx.doi.org/10.1111/gcb.13158>
- Lamont, K., Saintilan, N., Kelleway, J. J., Mazumder, D., & Zawadzki, A. (2020). Thirty-Year Repeat Measures of Mangrove Above- and Below-Ground Biomass Reveals Unexpectedly High Carbon Sequestration. *Ecosystems*, 23(2), 370-382. <https://doi.org/10.1007/s10021-019-00408-3>
- Craft, C., Clough, J., Ehman, J., Joye, S., Park, R., Pennings, S., Guo, H., & Machmuller, M. (2009). Forecasting the effects of accelerated sea-level rise on tidal marsh ecosystem services. *Frontiers in Ecology and the Environment*, 7(2), 73-78.
- Lovelock, C. E., Cahoon, D. R., Friess, D. A., Guntenspergen, G. R., Krauss, K. W., Reef, R., Rogers, K., Saunders, M. L., et al. (2015). The vulnerability of Indo-Pacific mangrove forests to sea-level rise. *Nature*, 526(7574), 559-563. Letter. <http://dx.doi.org/10.1038/nature15538>
- Ward, R. D., Friess, D. A., Day, R. H., & MacKenzie, R. A. (2016). Impacts of climate change on mangrove ecosystems: a region by region overview. *Ecosystem Health and Sustainability*, 2(4), e01211-n/a. <http://dx.doi.org/10.1002/ehs2.1211>
- Sandi, S. G., Rodríguez, J. F., Saintilan, N., Riccardi, G., & Saco, P. M. (2018). Rising tides, rising gates: The complex ecogeomorphic response of coastal wetlands to sea-level rise and human interventions. *Advances in Water Resources*, 114, 135-148. <http://www.sciencedirect.com/science/article/pii/S0309170817306164>
- Schuerch, M., Spencer, T., Temmerman, S., Kirwan, M. L., Wolff, C., Lincke, D., McOwen, C. J., Pickering, M. D., et al. (2018). Future response of global coastal wetlands to sea-level rise. *Nature*, 561(7722), 231-234. <https://doi.org/10.1038/s41586-018-0476-5>
- Mossman, H. L., Davy, A. J., & Grant, A. (2012). Does managed coastal realignment create saltmarshes with 'equivalent biological characteristics' to natural reference sites? *Journal of Applied Ecology*, 49(6), 1446-1456. <https://besjournals.onlinelibrary.wiley.com/doi/abs/10.1111/j.1365-2664.2012.02198.x>
- Hofstede, J. L. A. (2019). On the feasibility of managed retreat in the Wadden Sea of Schleswig-Holstein. *Journal of Coastal Conservation*, 23(6), 1069-1079. <https://doi.org/10.1007/s11852-019-00714-x>
- Elphick, C. S., Meiman, S., & Rubega, M. A. (2015). Tidal-flow restoration provides little nesting habitat for a globally vulnerable saltmarsh bird. *Restoration Ecology*, 23(4), 439-446. <https://onlinelibrary.wiley.com/doi/abs/10.1111/rec.12194>
- Boys, C. A., & Pease, B. (2017). Opening the floodgates to the recovery of nektonic assemblages in a temperate coastal wetland. *Marine and Freshwater Research*, 68(6), 1023-1035. <https://www.publish.csiro.au/paper/MF15445>
- Kroeger, K. D., Crooks, S., Moseman-Valtierra, S., & Tang, J. (2017). Restoring tides to reduce methane emissions in impounded wetlands: A new and potent Blue Carbon climate change intervention. *Scientific Reports*, 7(1), 11914. <https://doi.org/10.1038/s41598-017-12138-4>
- Sheehan, L., Sherwood, E. T., Moyer, R. P., Radabaugh, K. R., & Simpson, S. (2019). Blue Carbon: an Additional Driver for Restoring and Preserving Ecological Services of Coastal Wetlands in Tampa Bay (Florida, USA). *Wetlands*, 39(6), 1317-1328. <https://doi.org/10.1007/s13157-019-01137-y>

- Kelleway, J. J., Serrano, O., Baldock, J. A., Burgess, R., Cannard, T., Lavery, P. S., Lovelock, C. E., Macreadie, P. I., et al. (2020). A national approach to greenhouse gas abatement through blue carbon management. *Global Environmental Change*, 63, 102083. <http://www.sciencedirect.com/science/article/pii/S0959378019304017>
- Morris, J. T., Sundareshwar, P. V., Nietch, C. T., Kjerfve, B., & Cahoon, D. R. (2002). Responses of coastal wetlands to rising sea level. *Ecology*, 83(10), 2869-2877. [http://dx.doi.org/10.1890/0012-9658\(2002\)083\[2869:ROCWTRJ2.0.CO;2](http://dx.doi.org/10.1890/0012-9658(2002)083[2869:ROCWTRJ2.0.CO;2)
- Kirwan, M. L., Guntenspergen, G. R., D'Alpaos, A., Morris, J. T., Mudd, S. M., & Temmerman, S. (2010). Limits on the adaptability of coastal marshes to rising sea level. *Geophysical Research Letters*, 37(23), n/a-n/a. <http://dx.doi.org/10.1029/2010GL045489>
- Howe, A. J., Rodríguez, J. F., & Saco, P. M. (2009). Surface evolution and carbon sequestration in disturbed and undisturbed wetland soils of the Hunter estuary, southeast Australia. *Estuarine, Coastal and Shelf Science*, 84(1), 75-83. <http://www.sciencedirect.com/science/article/pii/S0272771409002856>
- Williams, R. J., Watford, F. A., & Balashov, V. (2000). *Kooragang Wetland Rehabilitation Project: History of Changes to Estuarine Wetlands of the Lower Hunter River*. Retrieved from Cronulla, Australia:
- Howe, A. J., Rodríguez, J. F., Spencer, J., MacFarlane, G. R., & Saintilan, N. (2010). Response of estuarine wetlands to reinstatement of tidal flows. *Marine and Freshwater Research*, 61(6), 702-713. <Go to ISI>://WOS:000279106700008
- Saintilan, N., & Williams, R. J. (1999). Mangrove Transgression into Saltmarsh Environments in South-East Australia. *Global Ecology and Biogeography*, 8(2), 117-124. <http://www.jstor.org/stable/2997853>
- Saintilan, N., Wilson, N. C., Rogers, K., Rajkaran, A., & Krauss, K. W. (2014). Mangrove expansion and salt marsh decline at mangrove poleward limits. *Global Change Biology*, 20(1), 147-157. <http://dx.doi.org/10.1111/gcb.12341>
- Kelleway, J. J., Cavanaugh, K., Rogers, K., Feller, I. C., Ens, E., Doughty, C., & Saintilan, N. (2017b). Review of the ecosystem service implications of mangrove encroachment into salt marshes. *Global Change Biology*. <http://dx.doi.org/10.1111/gcb.13727>
- Rogers, K., & Krauss, K. W. (2019). Moving from Generalisations to Specificity about Mangrove –Saltmarsh Dynamics. *Wetlands*, 39(6), 1155-1178. <https://doi.org/10.1007/s13157-018-1067-9>
- Rodríguez, J. F., & Howe, A. (2013). Estuarine Wetland Ecohydraulics and Migratory Shorebird Habitat Restoration. In I. Maddock, A. Harby, P. Kemp, & P. Wood (Eds.), *Ecohydraulics: an integrated approach* (pp. 375-394). Chichester, UK: John Wiley & Sons, Ltd.
- Riccardi, G. (2000). A cell model for hydrological-hydraulic modeling. *Journal of Environmental Hydrology*, 8.
- D'Alpaos, A., Lanzoni, S., Marani, M., & Rinaldo, A. (2007). Landscape evolution in tidal embayments: Modeling the interplay of erosion, sedimentation, and vegetation dynamics. *Journal of Geophysical Research: Earth Surface*, 112(F1), n/a-n/a. <http://dx.doi.org/10.1029/2006JF000537>
- Kirwan, M. L., & Murray, A. B. (2007). A coupled geomorphic and ecological model of tidal marsh evolution. *Proceedings of the National Academy of Sciences of the United States of America*, 104(15), 6118-6122. <http://www.ncbi.nlm.nih.gov/pmc/articles/PMC1851060/>
- Howe, A. (2008). *Hydrodynamics, geomorphology and vegetation of estuarine wetlands in the Hunter, Australia: implications for migratory shorebird high tide roost availability*. (PhD Thesis), University of Newcastle, Newcastle, Australia.
- Woodroffe, C. D., Rogers, K., McKee, K. L., Lovelock, C. E., Mendelssohn, I. A., & Saintilan, N. (2016). Mangrove Sedimentation and Response to Relative Sea-Level Rise. *Annual Review of Marine Science*, 8, 243-266.
- McKee, K. L. (1993). Soil Physicochemical Patterns and Mangrove Species Distribution--Reciprocal Effects? *Journal of Ecology*, 81(3), 477-487. <http://www.jstor.org.ezproxy.newcastle.edu.au/stable/2261526>
- Youssef, T., & Saenger, P. (1998). Photosynthetic gas exchange and accumulation of phytotoxins in mangrove seedlings in response to soil physico-chemical characteristics associated with waterlogging. *Tree Physiology*, 18(5), 317-324. <https://doi.org/10.1093/treephys/18.5.317>
- McKee, K. L. (1996). Growth and physiological responses of neotropical mangrove seedlings to root zone hypoxia. *Tree Physiology*, 16(11-12), 883-889. <https://doi.org/10.1093/treephys/16.11-12.883>
- van Maanen, B., Coco, G., & Bryan, K. R. (2015). On the ecogeomorphological feedbacks that control tidal channel network evolution in a sandy mangrove setting. *Proceedings of the Royal Society A: Mathematical, Physical and Engineering Science*, 471(2180). <http://rspa.royalsocietypublishing.org/content/royprsa/471/2180/20150115.full.pdf>
- Clarke, P. J., & Myerscough, P. J. (1993). The intertidal distribution of the grey mangrove (*Avicennia marina*) in southeastern Australia: The effects of physical conditions, interspecific competition, and predation on propagule establishment and survival. *Australian Journal of Ecology*, 18(3), 307-315. <https://onlinelibrary.wiley.com/doi/abs/10.1111/j.1442-9993.1993.tb00458.x>

- Cruse, B., Liedloff, A., Vesk, P. A., Burgman, M. A., & Wintle, B. A. (2013). Hydroperiod is the main driver of the spatial pattern of dominance in mangrove communities. *Global Ecology and Biogeography*, 22(7), 806-817. <http://dx.doi.org/10.1111/geb.12063>
- Krauss, K. W., Lovelock, C. E., McKee, K. L., López-Hoffman, L., Ewe, S. M. L., & Sousa, W. P. (2008). Environmental drivers in mangrove establishment and early development: A review. *Aquatic Botany*, 89(2), 105-127. <http://www.sciencedirect.com/science/article/pii/S0304377008000089>
- Saintilan, N., Rogers, K., & McKee, K. (2009). Salt Marsh-Mangrove Interactions in Australasia and the Americas. In G. M. E. Perillo, E. Wolanski, D. R. Cahoon, & M. M. Brinson (Eds.), *Coastal Wetlands - An Integrated Ecosystem Approach*. The Netherlands: Elsevier Science.
- Rogers, K., Saintilan, N., Howe, A. J., & Rodríguez, J. F. (2013). Sedimentation, elevation and marsh evolution in a southeastern Australian estuary during changing climatic conditions. *Estuarine, Coastal and Shelf Science*, 133, 172-181. <https://doi.org/10.1016/j.ecss.2013.08.025>
- Breda, A., Saco, P. M., Sandi, S. G., Saintilan, N., Riccardi, G., & Rodríguez, J. F. (2020). Accretion, retreat and transgression of coastal wetlands experiencing sea-level rise. *Hydrol. Earth Syst. Sci. Discuss.*, 2020, 1-22. <https://hess.copernicus.org/preprints/hess-2020-439/>
- Kirwan, M. L., & Guntenspergen, G. R. (2010). Influence of tidal range on the stability of coastal marshland. *Journal of Geophysical Research: Earth Surface*, 115(F2), n/a-n/a. <http://dx.doi.org/10.1029/2009JF001400>
- Kirwan, M. L., & Murray, A. B. (2008). Ecological and morphological response of brackish tidal marshland to the next century of sea level rise: Westham Island, British Columbia. *Global and Planetary Change*, 60(3-4), 471-486. <http://www.sciencedirect.com/science/article/pii/S0921818107001105>
- DPI, N. (2008). *Acid Sulfate Soils Priority Investigations for the Lower Hunter River Estuary*. Retrieved from Port Stephens.:
- Saintilan, N., Rogers, K., Mazumder, D., & Woodroffe, C. (2013). Allochthonous and autochthonous contributions to carbon accumulation and carbon store in southeastern Australian coastal wetlands. *Estuarine, Coastal and Shelf Science*, 128(Supplement C), 84-92. <http://www.sciencedirect.com/science/article/pii/S0272771413002333>
- Kauffman, J. B., & Donato, D. C. (2012). *Protocols for the measurement, monitoring and reporting of structure, biomass and carbon stocks in mangrove forests* (Vol. 86). Bogor, Indonesia: CIFOR.
- Owers, C. J., Rogers, K., & Woodroffe, C. D. (2018). Spatial variation of above-ground carbon storage in temperate coastal wetlands. *Estuarine, Coastal and Shelf Science*, 210, 55-67. <http://www.sciencedirect.com/science/article/pii/S0272771418300763>
- Negrin, V., Villalobos, A., González Trilla, G., Botté, S., & Marcovecchio, J. (2012). Above and belowground biomass and nutrient pools of *Spartina alterniflora* (smooth cordgrass) in a South American salt marsh. *Chemistry and Ecology*, 28(4). <https://doi.org/10.1080/02757540.2012.666529>
- Saintilan, N. (1997). Above- and below-ground biomasses of two species of mangrove on the Hawkesbury River estuary, New South Wales. *Marine and Freshwater Research*, 48(2), 147-152. <https://www.publish.csiro.au/paper/MF96079>
- Saintilan, N. (1998). Above- and below-ground biomass of mangroves in a sub-tropical estuary. *Marine and Freshwater Research*, 48(7), 601-604. <https://www.publish.csiro.au/paper/MF97009>
- Jaramillo, V. J., Kauffman, J. B., Rentería-Rodríguez, L., Cummings, D. L., & Ellingson, L. J. (2003). Biomass, Carbon, and Nitrogen Pools in Mexican Tropical Dry Forest Landscapes. *Ecosystems*, 6(7), 609-629. <https://doi.org/10.1007/s10021-002-0195-4>
- Duarte, C. M. (1990). Seagrass nutrient content. *Marine Ecology Progress Series*, 67, 201-207.
- Bouillon, S., Borges, A. V., Castañeda-Moya, E., Diele, K., Dittmar, T., Duke, N. C., Kristensen, E., Lee, S. Y., et al. (2008). Mangrove production and carbon sinks: A revision of global budget estimates. *Global Biogeochemical Cycles*, 22(2). <https://agupubs.onlinelibrary.wiley.com/doi/abs/10.1029/2007GB003052>
- Alongi, D. M. (2014). Carbon Cycling and Storage in Mangrove Forests. *Annual Review of Marine Science*, 6(1), 195-219. <https://doi.org/10.1146/annurev-marine-010213-135020>
- Krauss, K. W., Demopoulos, A. W. J., Cormier, N., From, A. S., McClain-Counts, J. P., & Lewis, R. R. (2018). Ghost forests of Marco Island: Mangrove mortality driven by belowground soil structural shifts during tidal hydrologic alteration. *Estuarine, Coastal and Shelf Science*, 212, 51-62. <http://www.sciencedirect.com/science/article/pii/S0272771418300519>
- Negandhi, K., Edwards, G., Kelleway, J. J., Howard, D., Safari, D., & Saintilan, N. (2019). Blue carbon potential of coastal wetland restoration varies with inundation and rainfall. *Scientific Reports*, 9(1), 4368. <https://doi.org/10.1038/s41598-019-40763-8>
- Church, J. A., Clark, P. U., Cazenave, A., Gregory, J. M., Jevrejeva, S., Levermann, A., Merrifield, M. A., Milne, G. A., et al. (2013). Sea Level Change. In T. F. Stocker, D. Qin, G.-K. Plattner, M. Tignor, S. K. Allen, J. Boschung, A. Nauels, Y. Xia, V. Bex, & P. M. Midgley (Eds.), *Climate Change 2013: The*

- Physical Science Basis. Contribution of Working Group I to the Fifth Assessment Report of the Intergovernmental Panel on Climate Change* (pp. 1137–1216). Cambridge, United Kingdom and New York, NY, USA: Cambridge University Press.
- Alizad, K., Hagen, S. C., Morris, J. T., Medeiros, S. C., Bilsie, M. V., & Weishampel, J. F. (2016b). Coastal wetland response to sea-level rise in a fluvial estuarine system. *Earth's Future*, 4(11), 483–497. <https://agupubs.onlinelibrary.wiley.com/doi/abs/10.1002/2016EF000385>
- Oppenheimer, M., Glavovic, B. C., Hinkel, J., van de Wal, R., Magnan, A. K., Abd-Elgawad, A., Cai, R., Cifuentes-Jara, M., et al. (2019). Sea Level Rise and Implications for Low-Lying Islands, Coasts and Communities. In H.-O. Pörtner, D. C. Roberts, V. Masson-Delmotte, P. Zhai, M. Tignor, E. Poloczanska, K. Mintenbeck, A. Alegría, M. Nicolai, A. Okem, J. Petzold, B. Rama, & N. M. Weyer (Eds.), *IPCC Special Report on the Ocean and Cryosphere in a Changing Climate*.
- Serrano, O., Lovelock, C. E., B. Atwood, T., Macreadie, P. I., Canto, R., Phinn, S., Arias-Ortiz, A., Bai, L., et al. (2019). Australian vegetated coastal ecosystems as global hotspots for climate change mitigation. *Nature Communications*, 10(1), 4313. <https://doi.org/10.1038/s41467-019-12176-8>
- Kauffman, J. B., Adame, M. F., Arifanti, V. B., Schile-Beers, L. M., Bernardino, A. F., Bhomia, R. K., Donato, D. C., Feller, I. C., et al. (2020). Total ecosystem carbon stocks of mangroves across broad global environmental and physical gradients. *Ecological Monographs*, 90(2), e01405. <https://esajournals.onlinelibrary.wiley.com/doi/abs/10.1002/ecm.1405>
- Duarte, C. M., Middelburg, J. J., & Caraco, N. (2005). Major role of marine vegetation on the oceanic carbon cycle. *Biogeosciences*, 2(1), 1–8. <https://www.biogeosciences.net/2/1/2005/>
- Lovelock, C. E., Adame, M. F., Bennion, V., Hayes, M., O'Mara, J., Reef, R., & Santini, N. S. (2014). Contemporary Rates of Carbon Sequestration Through Vertical Accretion of Sediments in Mangrove Forests and Saltmarshes of South East Queensland, Australia. *Estuaries and Coasts*, 37(3), 763–771. <https://doi.org/10.1007/s12237-013-9702-4>
- Horton, B. P., Shennan, I., Bradley, S. L., Cahill, N., Kirwan, M., Kopp, R. E., & Shaw, T. A. (2018). Predicting marsh vulnerability to sea-level rise using Holocene relative sea-level data. *Nature Communications*, 9(1), 2687. <https://doi.org/10.1038/s41467-018-05080-0>
- Törnqvist, T. E., Jankowski, K. L., Li, Y.-X., & González, J. L. (2020). Tipping points of Mississippi Delta marshes due to accelerated sea-level rise. *Science Advances*, 6(21), eaaz5512. <https://advances.sciencemag.org/content/advances/6/21/eaaz5512.full.pdf>
- Saintilan, N., Khan, N. S., Ashe, E., Kelleway, J. J., Rogers, K., Woodroffe, C. D., & Horton, B. P. (2020). Thresholds of mangrove survival under rapid sea level rise. *Science*, 368(6495), 1118–1121. <https://science.sciencemag.org/content/sci/368/6495/1118.full.pdf>
- Cameron, C., Hutley, L. B., Friess, D. A., & Brown, B. (2019). Community structure dynamics and carbon stock change of rehabilitated mangrove forests in Sulawesi, Indonesia. *Ecological Applications*, 29(1), e01810. <https://esajournals.onlinelibrary.wiley.com/doi/abs/10.1002/eap.1810>
- Liu, Y., Parolari, A. J., Kumar, M., Huang, C.-W., Katul, G. G., & Porporato, A. (2017). Increasing atmospheric humidity and CO₂ concentration alleviate forest mortality risk. *Proceedings of the National Academy of Sciences*, 114(37), 9918–9923. <https://www.pnas.org/content/pnas/114/37/9918.full.pdf>
- McKee, K. L., & Rooth, J. E. (2008). Where temperate meets tropical: multi-factorial effects of elevated CO₂, nitrogen enrichment, and competition on a mangrove-salt marsh community. *Global Change Biology*, 14(5), 971–984. <https://onlinelibrary.wiley.com/doi/abs/10.1111/j.1365-2486.2008.01547.x>
- Howard, R. J., Stagg, C. L., & Utomo, H. S. (2018). Early growth interactions between a mangrove and an herbaceous salt marsh species are not affected by elevated CO₂ or drought. *Estuarine, Coastal and Shelf Science*, 207, 74–81. <http://www.sciencedirect.com/science/article/pii/S0272771417309095>
- Reef, R., Winter, K., Morales, J., Adame, M. F., Reef, D. L., & Lovelock, C. E. (2015). The effect of atmospheric carbon dioxide concentrations on the performance of the mangrove *Avicennia germinans* over a range of salinities. *Physiologia Plantarum*, 154(3), 358–368. <https://onlinelibrary.wiley.com/doi/abs/10.1111/ppl.12289>
- Ball, M. C., Cochrane, M. J., & Rawson, H. M. (1997). Growth and water use of the mangroves *Rhizophora apiculata* and *R. stylosa* in response to salinity and humidity under ambient and elevated concentrations of atmospheric CO₂. *Plant, Cell & Environment*, 20(9), 1158–1166. <https://onlinelibrary.wiley.com/doi/abs/10.1046/j.1365-3040.1997.d01-144.x>
- Arp, W. J., Drake, B. G., Pockman, W. T., Curtis, P. S., & Whigham, D. F. (1993). Interactions between C₃ and C₄ Salt Marsh Plant Species during Four Years of Exposure to Elevated Atmospheric CO₂. *Vegetatio*, 104/105, 133–143. <https://www.jstor.org/stable/20029742>
- Ratliff, K. M., Braswell, A. E., & Marani, M. (2015). Spatial response of coastal marshes to increased atmospheric CO₂. *Proceedings of the National Academy of Sciences*, 112(51), 15580–15584. <https://www.pnas.org/content/pnas/112/51/15580.full.pdf>

- Cahoon, D. R., McKee, K. L., & Morris, J. T. (2020). How Plants Influence Resilience of Salt Marsh and Mangrove Wetlands to Sea-Level Rise. *Estuaries and Coasts*. <https://doi.org/10.1007/s12237-020-00834-w>
- Chen, R., & Twilley, R. R. (1998). A gap dynamic model of mangrove forest development along gradients of soil salinity and nutrient resources. *Journal of Ecology*, 86(1), 37-51. <https://besjournals.onlinelibrary.wiley.com/doi/abs/10.1046/j.1365-2745.1998.00233.x>

Accelerated Sea-Level Rise Limits Vegetation Capacity to Sequester Carbon in Coastal Wetlands

S.G. Sandi¹, P.M. Saco¹, N. Saintilan², G. Riccardi³, and J.F. Rodriguez¹

¹ Centre for Water Security and Environmental Sustainability and School of Engineering, The University of Newcastle, Australia

² Department of Environmental Sciences, Macquarie University, Australia

³ Department of Hydraulics and Research Council of National University of Rosario (CIUNR), Argentina

Contents of this file

Text S1

Figures S1 to S6

Tables S1 to S4

Introduction

This supporting information provides a description of soil carbon sampling methods, results from hydrodynamic and vegetation models calibration, parameters calibrated for the eco-geomorphic accretion model, results from using a simplified bathtub approach, soil carbon soil carbon profiles in the region and synthetic soil carbon profiles calculated for the study site.

Text S1. Soil carbon sampling in Area E.

Soil carbon densities (ρ_{sd}) in Area E were obtained for the top 20 cm of the top soil layer of different vegetated and non-vegetated areas by extracting 45 different soil cores (Howe et al., 2009). Core samples were obtained by inserting a 5.5 cm diameter, 25 cm long polyvinyl chloride tube to a depth of 20 cm. In the laboratory, length and mass of the core samples were measured and then samples were air dried to obtain dry bulk density. Soil was then sieved with a fine mesh to remove the fine root material and soil samples were selected from the sieved soil forming samples of less than 1 g. Samples were treated with HCl to remove carbonates, and total carbon and organic carbon was determined with a LECO CNS 2000 analyser. Mean organic soil carbon densities were $0.0406 \text{ MgC}\cdot\text{m}^{-3}$ (SD = $0.010 \text{ MgC}\cdot\text{m}^{-3}$, n = 19) for saltmarsh, $0.0287 \text{ MgC}\cdot\text{m}^{-3}$ (SD = $0.009 \text{ MgC}\cdot\text{m}^{-3}$, n = 9) for mangrove, and $0.0193 \text{ MgC}\cdot\text{m}^{-3}$ (SD = $0.006 \text{ MgC}\cdot\text{m}^{-3}$, n = 8) for unvegetated tidal pools and mudflats.

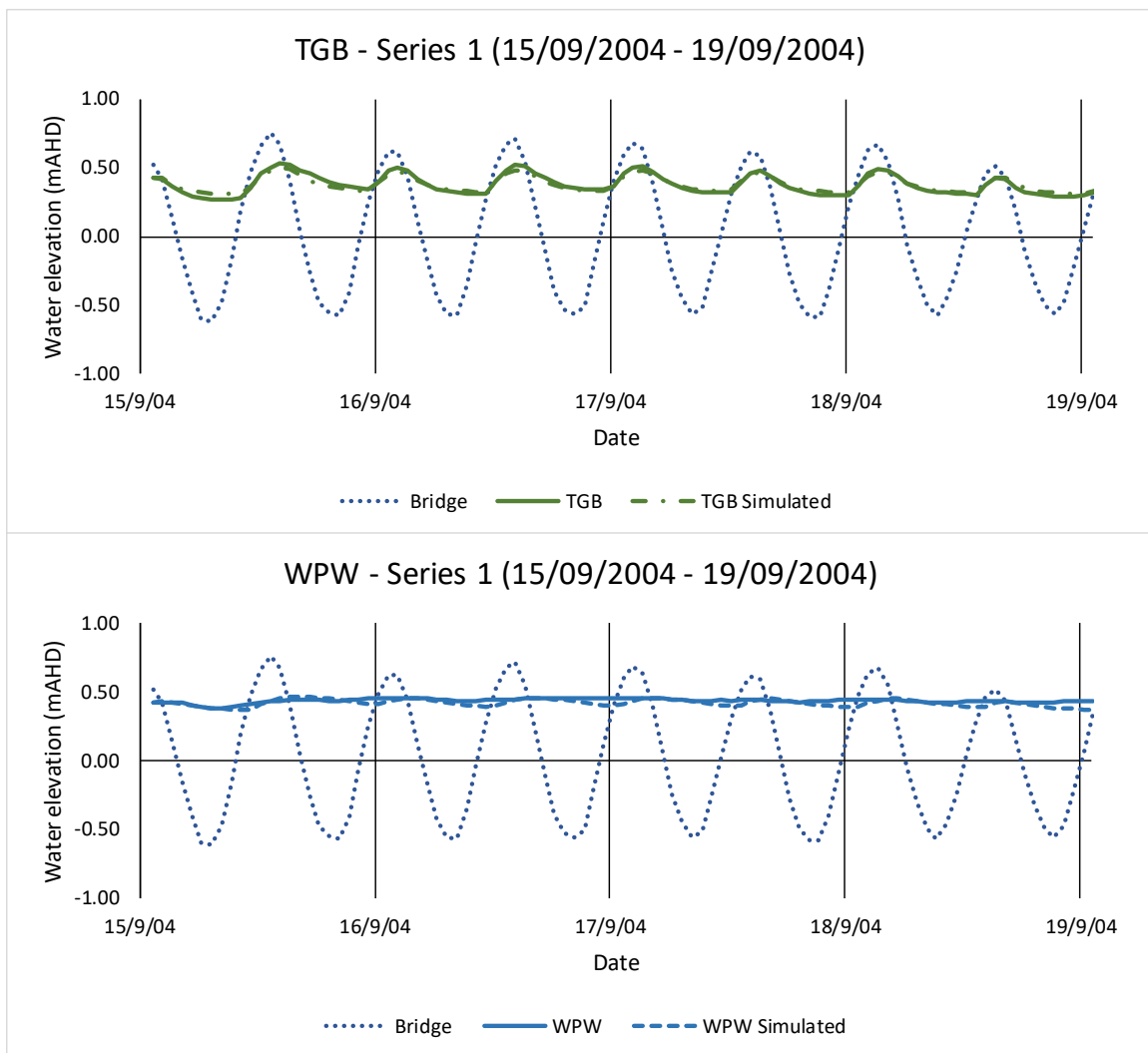


Figure S1. Comparison plot of simulated water levels for Series 1 at locations TGB and WPW. Input water level at Bridge location is also presented.

Note: Adapted from Sandi et al. (2018).

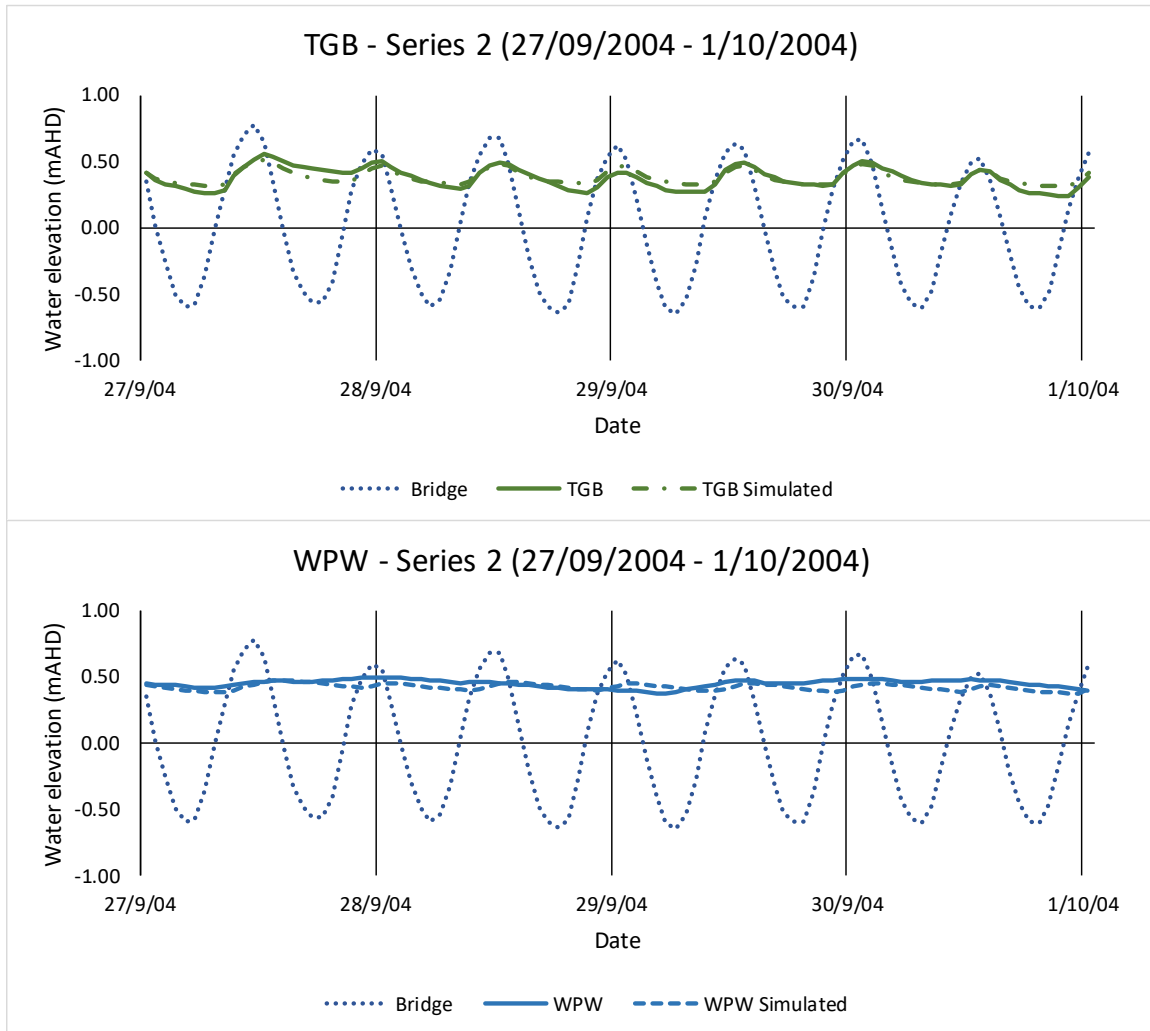


Figure S2. Comparison plot of simulated water levels for Series 2 at locations TGB and WPW. Input water level at Bridge location is also presented.

Note: Adapted from Sandi et al. (2018).

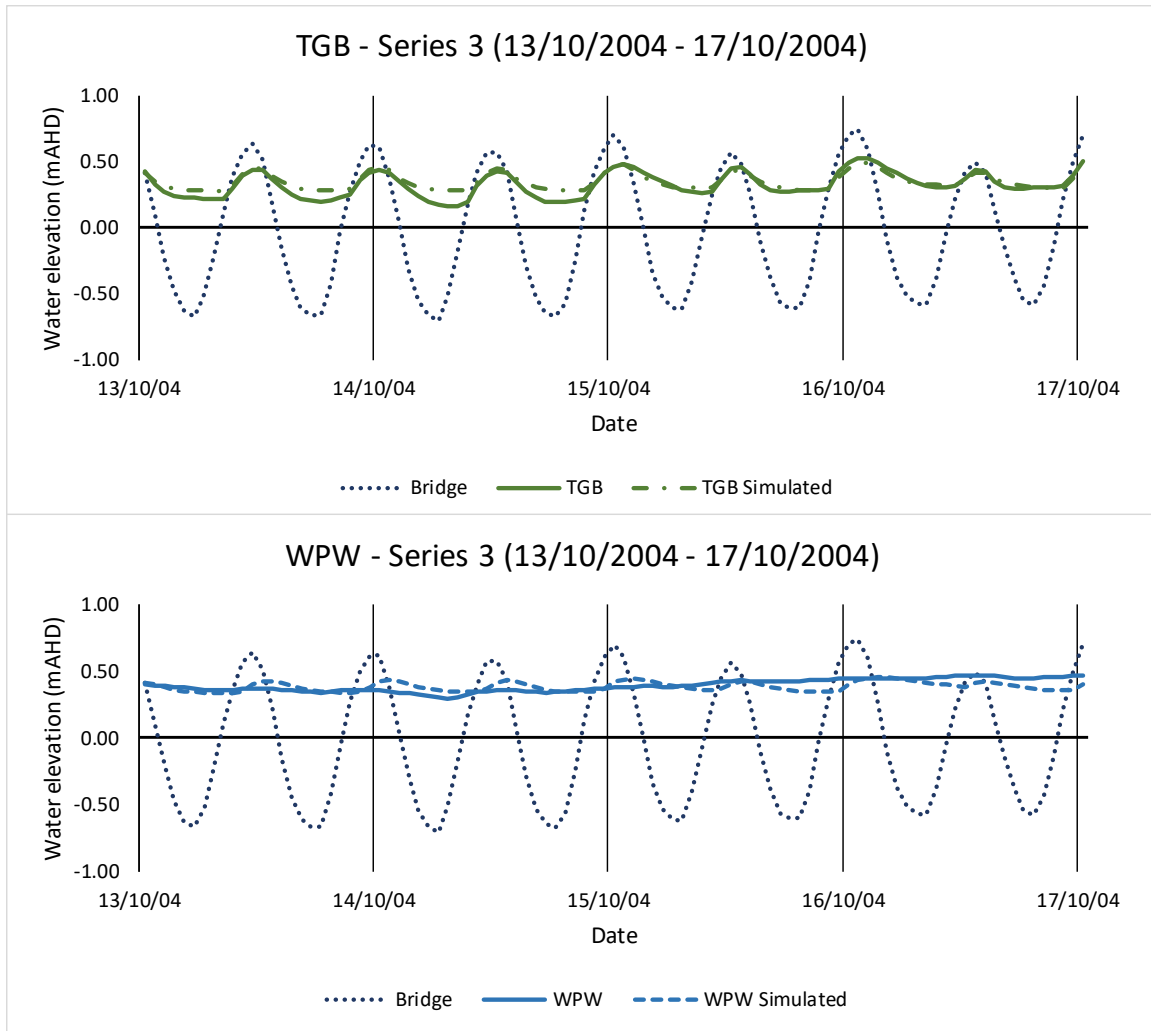


Figure S3. Comparison plot of simulated water levels for Series 3 at locations TGB and WPW. Input water level at Bridge location is also presented.

Note: Adapted from Sandi et al. (2018).

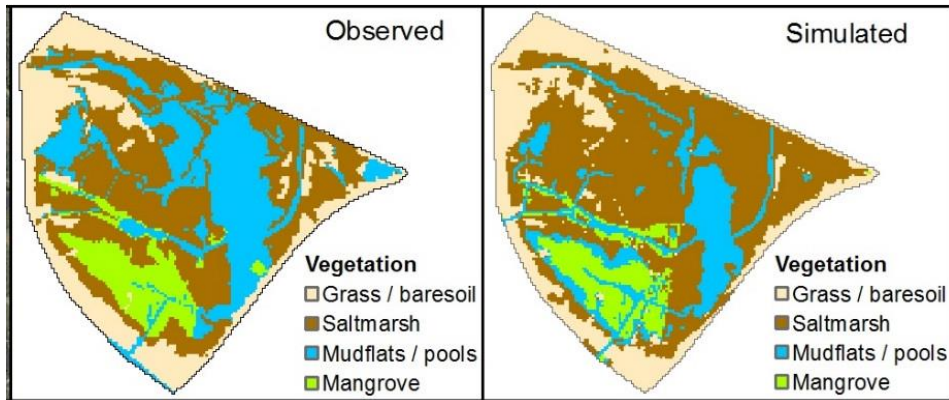


Figure S4. Comparison of observed and simulated vegetation in Area E.
Note: based on data from Rodríguez et al. (2017).

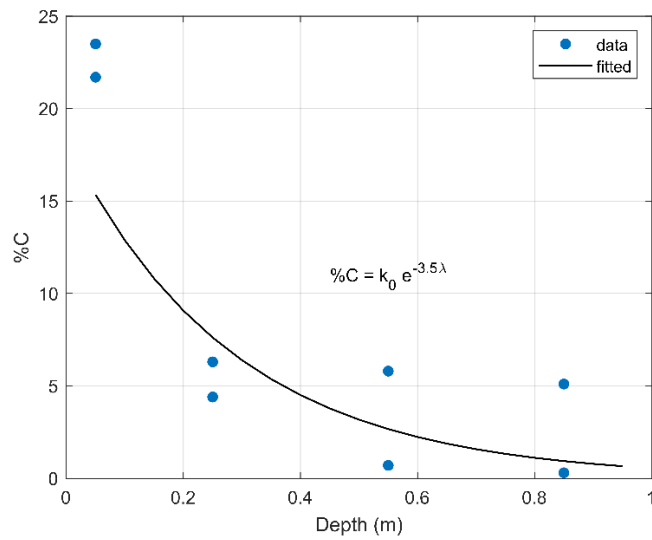


Figure S5. Soil carbon profile to 1 m depth.
Note: based on data from Saintilan et al. (2013).

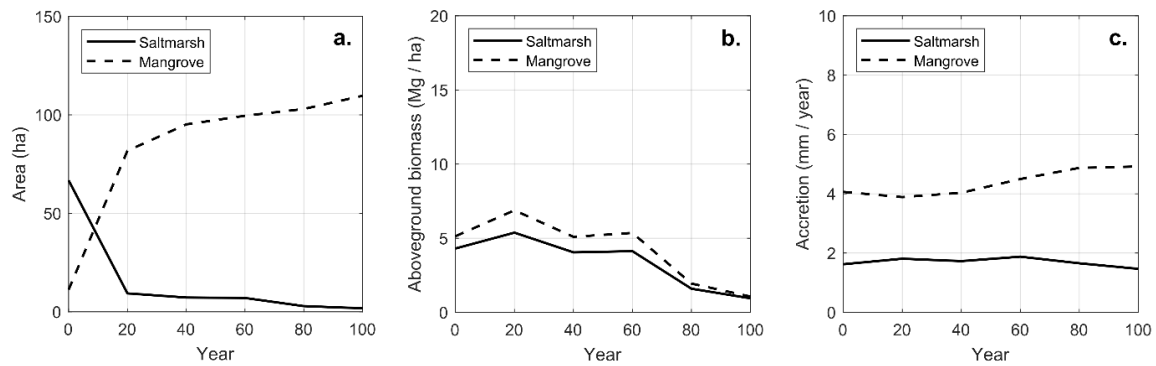


Figure S6. Simulated changes in vegetation extent in ha (a), aboveground biomass in $\text{MgC} \cdot \text{ha}^{-1}$ (b), and accretion rates in $\text{mm} \cdot \text{year}^{-1}$ (c) using a bathtub mode.

Table S1. Model performance for 3 water depth time series used in calibration and model testing of the hydrodynamic model.

Series and location		RSR	PBIAS (%)	NS
S1 Calibration (15/09/2004) – (19/09/2004)	TGB	0.03 (Excellent)	-0.29 (Excellent)	0.99 (Excellent)
	WPW	0.04 (Excellent)	3.68 (Excellent)	0.99 (Excellent)
S2 model testing (27/09/2004) – (01/10/2004)	TGB	0.06 (Excellent)	-1.69 (Excellent)	0.99 (Excellent)
	WPW	0.05 (Excellent)	6.04 (Excellent)	0.99 (Excellent)
S3 model testing (13/10/2004) – (17/09/2004)	TGB	0.08 (Excellent)	-6.96 (Excellent)	0.99 (Excellent)
	WPW	0.07 (Excellent)	2.27 (Excellent)	0.99 (Excellent)

Note: based on data from Sandi et al. (2018).

Table S2. General confusion matrix for evaluation of vegetation prediction model.

	Predicted: Other	Predicted: Saltmarsh	Predicted: Mangrove	
Observed: Other	4518	2410	77	7005
Observed: Saltmarsh	946	4160	206	5312
Observed: Mangrove	278	108	840	1226
	5742	6678	1123	

Note: based on data from Sandi et al. (2018).

Table S3. Parameters for eco-geomorphic accretion model.

Model parameters	Saltmarsh	Mangrove
Average depth below mean high tide D (m)	0.142	0.474
Average suspended sediment concentration SSC (g/m ³)	15	22
Average aboveground biomass production B (g/m ² /year)	900	1000
Average surface elevation change dE/dt (m/year)	0.00139	0.00223
Equation 1	$\frac{dE}{dt} = SSC(q + kB)D$	
Sediment entrapment rate k (m ⁵ /g ²)	6.2x10 ⁻⁷	1.2x10 ⁻⁷
Sediment settling rate q (m ³ /year)	0.00009	0.00009
Equation 2	$B = aD + bD^2 + c$	
Empirical parameters		
a (g/m ³ /year)	8384	7848
b (g/m ⁴ /year)	-16767	-6038
c (g/m ² /year)	0	-1328
Maximum B (g/m ² /year)	1050	1223

Note: based on data from Rodríguez et al. (2017) and Sandi et al. (2018).

Table S4. Soil organic carbon density (Mg C /m³) profiles for different habitats in Area E.

	Organic carbon density (Mg C /m ³)		
Soil depth	Saltmarsh	Mudflat / pool	Mangrove
0 – 20	0.0406	0.0193	0.0287
20 – 40	0.0202	0.0096	0.0143
40 – 60	0.01	0.0048	0.0071
60 – 80	0.005	0.0024	0.0035
80 – 100	0.0025	0.0012	0.0017

References

- Howe, A. J., Rodríguez, J. F., & Saco, P. M. (2009). Surface evolution and carbon sequestration in disturbed and undisturbed wetland soils of the Hunter estuary, southeast Australia. *Estuarine, Coastal and Shelf Science*, 84(1), 75-83.
<http://www.sciencedirect.com/science/article/pii/S0272771409002856>
- Rodríguez, J. F., Saco, P. M., Sandi, S., Saintilan, N., & Riccardi, G. (2017). Potential increase in coastal wetland vulnerability to sea-level rise suggested by considering hydrodynamic attenuation effects. *Nature Communications*, 8, 16094. Article.
<http://dx.doi.org/10.1038/ncomms16094>
- Saintilan, N., Rogers, K., Mazumder, D., & Woodroffe, C. (2013). Allochthonous and autochthonous contributions to carbon accumulation and carbon store in southeastern Australian coastal wetlands. *Estuarine, Coastal and Shelf Science*, 128(Supplement C), 84-92.
<http://www.sciencedirect.com/science/article/pii/S0272771413002333>
- Sandi, S. G., Rodríguez, J. F., Saintilan, N., Riccardi, G., & Saco, P. M. (2018). Rising tides, rising gates: The complex ecogeomorphic response of coastal wetlands to sea-level rise and human interventions. *Advances in Water Resources*, 114, 135-148. <http://www.sciencedirect.com/science/article/pii/S0309170817306164>